Supporting Information

Establishing PQ-ERA Photoclick Reactions with Unprecedented Efficiency by Engineering of the Nature of the Phenanthraquinone Triplet State

Youxin Fu,[a] Georgios Alachouzos,[a] Nadja A. Simeth,[a,b] Mariangela Di Donato,[c,d] Michiel F. Hilbers,[e] Wybren Jan Buma,[e,f,*] Wiktor Szymanski,[a,g,*] and Ben L. Feringa[a,*]

[a]Centre for Systems Chemistry, Stratingh Institute for Chemistry, Faculty for Science and Engineering, University of Groningen, Nijenborgh 4, 9747 AG Groningen, The Netherlands.

[b]current address: Institute for Organic and Biomolecular Chemistry, Georg-August-University Göttingen, Tammanstraße 2, 37077 Göttingen, Germany.

[c]LENS (European Laboratory for Non-Linear Spectroscopy), via N. Carrara 1, 50019 Sesto Fiorentino (FI), Italy;

[d]ICCOM-CNR, via Madonna del Piano 10, 50019 Sesto Fiorentino (FI), Italy.

[e]Van 't Hoff Institute for Molecular Sciences, University of Amsterdam Science Park 904, 1098 XH Amsterdam, The Netherlands.

[f] Institute for Molecules and Materials, FELIX Laboratory, Radboud University, Toernooiveld 7c, 6525 ED Nijmegen, The Netherlands.

[g]Department of Radiology, Medical Imaging Center, University of Groningen, University Medical Centre Groningen, Hanzeplein 1, 9713 GZ Groningen, The Netherlands.

Table of Contents

1. General Information

Synthesis and isolation. Solvents used were of analytical grade. All other chemicals were used as received unless otherwise indicated. Deionized water was used throughout. All oxygen or moisture-sensitive reactions were performed in dried glassware and under N_2 atmosphere using standard Schlenk techniques. Dry solvents were obtained from an MBraun solvent purification system (SPS). Column chromatography was performed on silica gel (Silica 60 M, 0.04-0.063 mm.

Reaction monitoring. Reactions were monitored using thin-layer chromatography (TLC) on aluminium sheets coated with silica gel 60 F254 (MERCK). Components were visualized by UV-light (254 nm, 365 nm) and potassium permanganate or Seebach staining. Alternatively, the progress of the reaction and conversion were determined by UPLC-MS, using a Thermo Fisher Scientific Vanquish UPLC System on a C18 column with a LCQ Fleet ion trap mass spectrometer.

Analysis. Mass spectra were recorded on an AEI-MS-902 mass spectrometer (EI+) or a LTQ Orbitrap XL (ESI+, ESI-, APCI+). ^{1}H- and ^{13}C NMR were recorded on Bruker AM-400 Spectrometer (400 MHz and 100.59 MHz, respectively), or a Varian AMX400 (400 MHz and 100.59 MHz, respectively), a 300 MHz (300 MHz and 75 MHz, respectively for ^{1}H- and ^{13}C-NMR) using DMSO-d_6 as solvent. Data are reported as follows: chemical shifts, multiplicity (s = singlet, d = doublet, t = triplet, q = quartet, m = multiplet), coupling constants (Hz), and integration. UV-Vis spectra were recorded on a Hewlett-Packard HP 8543 Diode Array, an Agilent 8453 UV-Visible spectrophotometer in a quartz cuvette with 1 cm pathlength at 20 °C. Fluorescence and fluorescence quantum yield measurements were performed on a Edinburgh instruments FS5 spectrofluorometer. The Agilent 8453 UV-Visible spectrometer was equipped with a custom-built (Prizmatix/Mountain Photonics) multi-wavelength fiber coupled LED-system (FC6-LED-WL) including the following LEDs: 365A, 390B, 420Z, 445B, 535R, 630CA. The emission profile of LEDs can be found: https://www.prizmatix.com/FC/Multi-

Wavelength-Fiber-Coupled-LEDs.aspx. A detailed description of the setup was published earlier by our group (see Figure S1).[1] A Quantum Northwest TC1 temperature controller was used to maintain the temperature at 20 °C during photochemical studies.

Femtosecond Transient Absorption Spectroscopy. The apparatus used for the transient absorption spectroscopy (TAS) measurements has been described in detail before. Briefly, 40 fs pulses centred at 800 nm, were produced by an integrated Ti:sapphire oscillator (Micra-Coherent) coupled with a regenerative amplifier system (Legend-Coherent). The excitation wavelength was set at 400 nm and excitation power was set at about 200 nJ for all measurements. The pump pulses were generated by second harmonic generation of the fundamental laser radiation using a 2 mm thick BBO crystal. The white light probe pulse was generated by focusing a small portion of the fundamental laser radiation on a 3 mm thick CaF_2 window. A portion of the generated white light was sent to the sample through a different path and used as a reference signal. After passing through the sample the white light probe and reference pulses were both directed to a flat field monochromator coupled to a home-made detector. Transient signals were acquired in a time interval spanning up to 1500 ps. The sample was contained in a 2 mm quartz cuvette, mounted on a movable holder to minimize photodegradation. Measurements were performed at room temperature. Concentrations were adjusted to an absorbance of 0.9 – 1.0 OD (for the respective optical path) at the absorption maximum which amounted to about 0.3 – 0.5 OD at excitation wavelength. Before and after the measurements, the integrity of the sample was checked on a PerkinElmer LAMBDA 950 spectrophotometer. The data have been analysed by global analysis using the software Glotaran (Snellenburg, J. J., Laptenok, S., Seger, R., Mullen, K. M., & van Stokkum, I. H. M. (2012).[2]

Nanosecond Transient Absorption Spectroscopy. Nanosecond transient absorption spectra were recorded with an in-house assembled setup with 400 nm used as the excitation wavelength for all of the samples. The excitation wavelength was generated using a tunable Nd: YAG-laser system (NT342B, Ekspla) comprising the pump laser (NL300) with harmonics generators

(SHG, THG) producing 355 nm to pump an optical parametric oscillator (OPO) with SHG connected in a single device. The laser system was operated at a repetition rate of 10 Hz with a pulse length of 5 ns. The probe light running at 20 Hz was generated by a high-stability short arc xenon flash lamp (FX-1160, Excelitas Technologies) using a modified PS302 controller (EG&G). Using a 50/50 beam splitter, the probe light was split equally into a signal beam and a reference beam and focused (bi-convex lens 75mm) on the entrance slit of a spectrograph (SpectraPro-150, Princeton Instruments) with a grating of 150 ln/mm, blaze at 500 nm. The probe beam (A = 1 mm^2) was passed through the sample cell and orthogonally overlapped with the excitation beam on a 1 mm × 1 cm area. The excitation energy was recorded by measuring the excitation power at the back of an empty sample holder. In order to correct for fluctuations in the flash lamp spectral intensity, the reference was used to normalize the signal. Both beams were recorded simultaneously using a gated intensified CCD camera (PI-MAX3, Princeton Instruments) which has an adjustable gate of minimal 2.9 ns, normally a gate of 20 ns and software binning is used to improve the dynamic range and signal to noise ratio. Two delay generators (DG535 and DG645, Stanford Research Systems, Inc.) were used to trigger the excitation and to change the delay of the flash lamp together with the gate of the camera during the experiment. The setup was controlled by an in-house written Labview program.

Computational methods. Geometry optimization of **PQ**, **PQ-3TP** and **PQ-3DiTP** followed by calculation of harmonic force fields was performed for the electronic ground state and electronically excited triplet states using (Time Dependent) Density Functional Theory (TD-DFT). Solvent effects were taken into account using the Polarizable Continuum Model (PCM) with the appropriate parameters for acetonitrile. These calculations have been performed using various functionals and basis sets (M06-2X/6-31+G*, wb97XD/cc-pVDZ, and MN15/def2TZVP)[3–8] but only minor differences were found between them. All calculations have been performed with the Gaussian16, Rev. C.01 suite of programs.[9]

Photocycloaddition of PQs with traps in solution. Stock solutions of **PQs** (10 mM), and *N*-boc-2,3-dihydro-1*H*-pyrrole (**PY**, 100 mM), in DMSO were prepared. From them, a solution of **PQs/PY** (50/500) was prepared in MeCN (2.5 mL) in a quartz cuvette and degassed by N_2 for 3 min. 365nm (365A), 390 nm LED (390B), 420nm (420Z), and 445 nm LED (445B) were used as light source for photoclick reactions and positioned at a fixed distance to the cuvette. Changes in the absorption were monitored every 1 s.

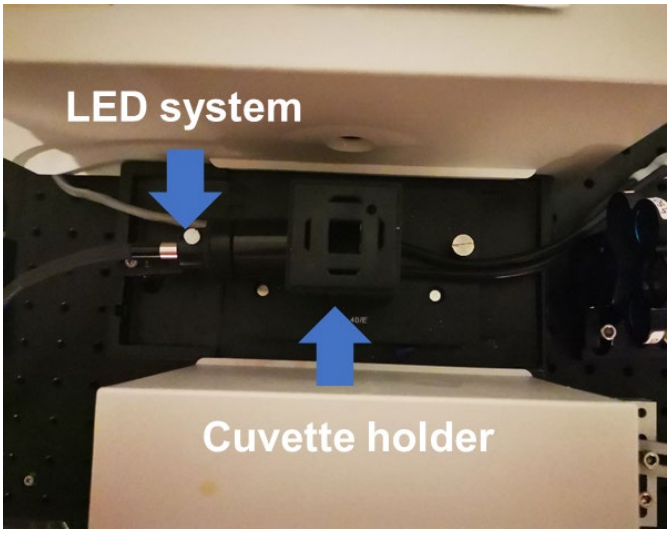

Fig. S1. Photograph of LED-system (FC6-LED-WL).

2. Synthesis of PQ compounds and photoclick products

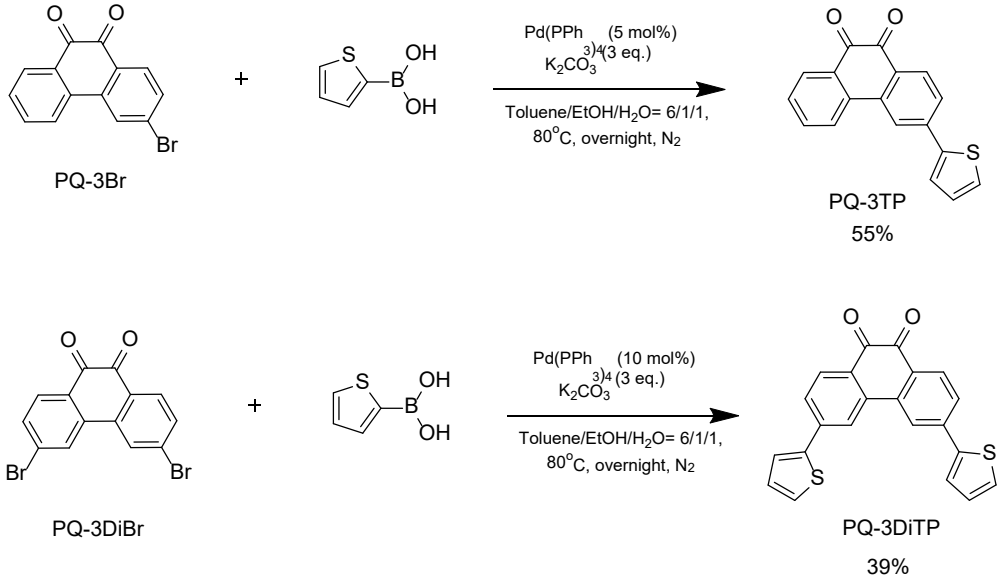

Scheme S1. Synthesis of **PQ** derivatives.

2.1. Synthesis of compound PQ-3TP

A Schlenk tube containing 3-bromophenanthrene-9,10-dione (**PQ-3Br**, 200 mg, 0.7 mmol), and 2-thienylboronic acid (98 mg, 0.77 mmol), and $Pd(PPh_3)_4$ (46 mg, 0.04 mmol) was evacuated and backfilled with N_2 for three times. After the addition of degassed K_2CO_3 solution (304 mg in 3.5 mL H_2O), ethanol (4 ml), and toluene (15 mL), the tube was sealed under N_2 atmosphere and heated at 80 ºC for 12 h. After being cooled to room temperature, the reaction mixture was diluted with dichloromethane, the phases were separated and the organic layer was washed with water and dried over anhydrous Na_2SO_4. Upon removal of solvents in vacuo, the residual was purified by column chromatography over silica gel eluted with ethyl acetate/dichloromethane (1/5, v/v) to obtain **PQ-3TP** as an orange solid in 55% yield (0.42 mmol, 111 mg). ^{1}H NMR (400 MHz, DMSO-d_6) δ 8.52 (d, J = 6.3 Hz, 2H), 8.07 – 8.01 (m, 2H), 8.00 (d, J = 3.5 Hz, 1H), 7.81 (t, J = 7.7 Hz, 1H), 7.78 – 7.74 (m, 2H), 7.56 (t, J = 7.5 Hz, 1H), 7.26 (dd, J = 5.0, 3.7 Hz, 1H). ^{13}C NMR (101 MHz, DMSO-d_6) δ 178.8, 142.2, 136.1, 130.9, 129.5, 129.0, 127.7, 126.8, 121.3. HR-MS (ESI) *m/z*, calculated for $[M+H]^+$: 291.0474 ; found: 291.0474.

2.2. Synthesis of compound PQ-3DiTP

The title compound was synthesized using the same method as for **PQ-3TP**, employing 3,6-dibromophenanthrene-9,10-dione (**PQ-3DIBr**, 200 mg, 0.55 mmol) and 2-thienylboronic acid (173 mg, 1.37 mmol) to obtain **PQ-3DiTP** as orange solid in 39% yield (0.21 mmol, 80 mg). ^{1}H NMR (400 MHz, DMSO-d_6) δ 8.60 (s, 2H), 8.08 – 8.01 (m, 4H), 7.79 – 7.72 (m, 4H), 7.30 – 7.23 (m, 2H). ^{13}C NMR (101 MHz, DMSO-d_6) δ 178.8, 142.2, 136.1, 130.8, 129.4, 129.0, 127.7, 126.7, 121.2. HR-MS (ESI) *m/z*, calculated for $[M+Na]^+$: 395.0171 ; found: 395.0170.

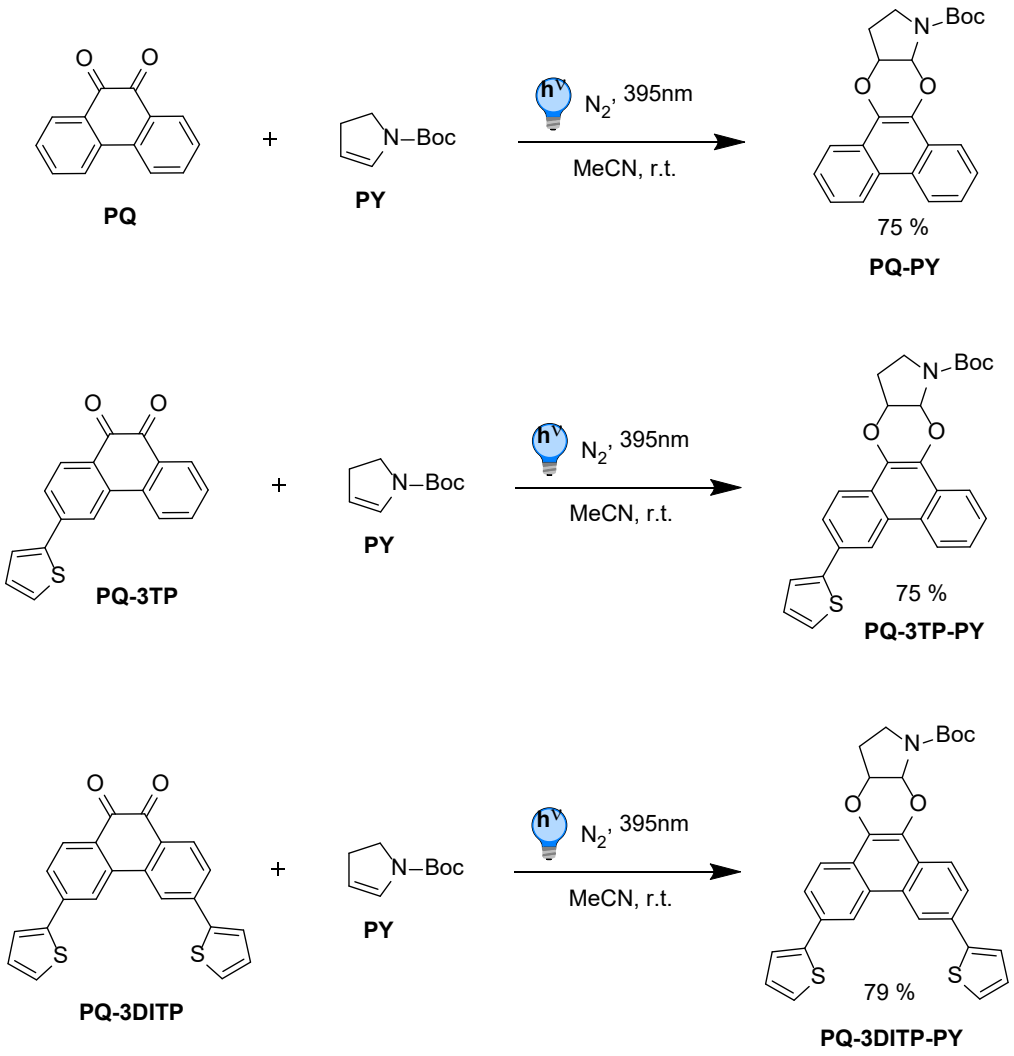

Scheme S2. Synthesis of **PQs-PY** derivatives (as a mixture of two regioisomers).

2.3. Synthesis of PQ-PY

PQ (0.2 mmol, 40 mg) and **PY** (1 mmol, 174 mg) were dissolved in 20 mL MeCN. Then, the reaction mixture was stirred and irradiated using hand-held LED lamp (395 nm, 88 mW cm^{-2}) at a fixed distance for 1 min under N_2 atmosphere. The reaction was monitored by TLC. After full consumption of **PQ**, the volatiles were evaporated and the resulting residue was purified by column chromatography on silica gel (dichloromethane/ethyl acetate = 1:4, v/v) to afford **PQ-PY** as a colorless powder (54 mg, 0.14 mmol, 75 % yield). ^{1}H NMR (400 MHz, DMSO-d_6) δ 8.73 (d, J = 8.2 Hz, 2H), 8.05 (t, J = 6.6 Hz, 2H), 7.67 – 7.54 (m, 4H), 5.65 (s, 1H), 5.13 (ddd, J = 10.4, 6.8, 3.9 Hz, 1H), 3.50 (t, J = 9.6 Hz, 1H), 2.34 (dt, J = 12.2, 7.0 Hz, 1H), 2.02 – 1.90 (m, 1H), 1.48 (s, 9H). ^{13}C NMR (101 MHz, DMSO-d_6) δ 153.7, 127.5, 126.7, 126.6, 125.8, 125.7, 123.4, 120.7, 80.5, 28.5. HR-MS (ESI) *m/z*, calculated for $[M+Na]^+$: 400.1529; found: 400.1526.

2.4. Synthesis of PQ-3TP-PY

The title compound was synthesized using the same method as for **PQ-PY**, employing **PQ-3TP** (0.1 mmol, 30 mg) to afford **PQ-3TP-PY** as a colorless powder (34 mg, 0.075 mmol, 75 % yield). ^{1}H NMR (400 MHz, DMSO-d_6) δ 8.96 (s, 1H), 8.90 (d, J = 8.2 Hz, 1H), 8.08 (q, J = 6.8, 5.2 Hz, 2H), 7.92 (dd, J = 8.5, 1.5 Hz, 1H), 7.82 (d, J = 3.5 Hz, 1H), 7.72 – 7.57 (m, 3H), 7.23 – 7.17 (m, 1H), 5.72 – 5.64 (m, 1H), 5.20 – 5.12 (m, 1H), 3.58 – 3.49 (m, 1H), 3.47 – 3.37 (m, 1H), 2.42 – 2.32 (m, 1H), 2.05 – 1.93 (m, 1H), 1.50 (s, 9H). ^{13}C NMR (101 MHz, DMSO-d_6) δ 153.7, 143.9, 131.3, 129.2, 127.8, 127.2, 126.5, 126.3, 125.8, 125.3, 124.8, 123.8, 121.7, 120.8, 119.5, 80.6, 28.5. HR-MS (ESI) *m/z*, calculated for $[M+Na]^+$: 482.1397; found: 482.1395.

2.5. Synthesis of PQ-3DiTP-PY

The title compound was synthesized using the same method as for **PQ-PY**, employing **PQ-3DiTP** (0.1 mmol, 37 mg) to afford **PQ-3DiTP-PY** as a colorless powder (43 mg, 0.079 mmol, 79 % yield). ^{1}H NMR (400 MHz, DMSO-d_6) δ 9.06 (s, 2H), 8.10 (t, J = 8.4 Hz, 2H), 7.99 –

7.87 (m, 4H), 7.62 (d, J = 5.0 Hz, 2H), 7.25 – 7.19 (m, 2H), 5.69 (s, 1H), 5.18 (ddd, J = 10.5, 6.8, 4.1 Hz, 1H), 3.54 (t, J = 9.7 Hz, 1H), 3.49 – 3.38 (m, 1H), 2.43 – 2.34 (m, 1H), 2.08 – 1.94 (m, 1H), 1.51 (s, 10H). ^{13}C NMR (101 MHz, DMSO-d_6) δ 153.7, 143.9, 143.8, 131.4, 131.3, 129.1, 129.0, 127.0, 126.9, 126.4, 126.3, 125.7, 125.2, 125.1, 125.0, 121.8, 119.7, 80.6, 28.5. HR-MS (ESI) *m/z*, calculated for $[M+Na]^+$: 482.1397; found: 482.1395.

3. NMR Spectra

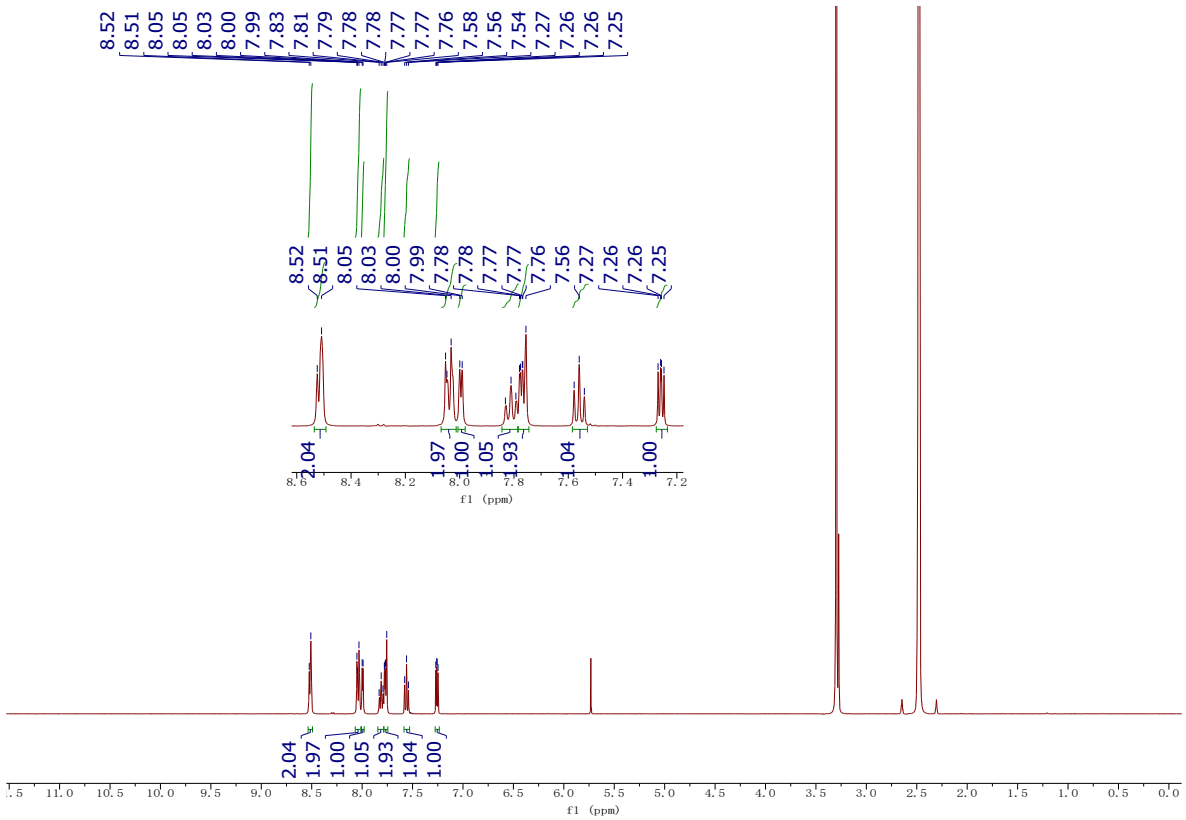

Fig. S3. [1]H NMR of **PQ-3TP** in DMSO-d_6.

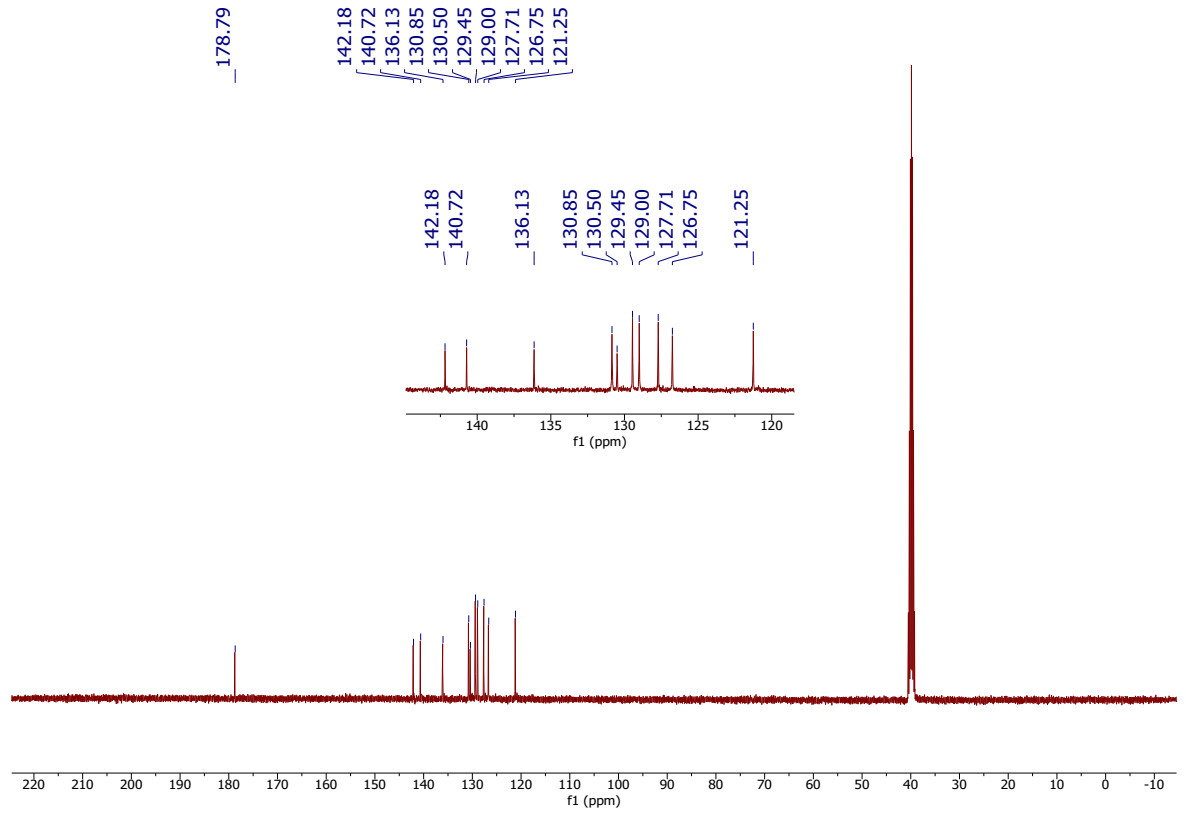

Fig. S4. [13]C NMR of **PQ-3TP** in DMSO-d_6.

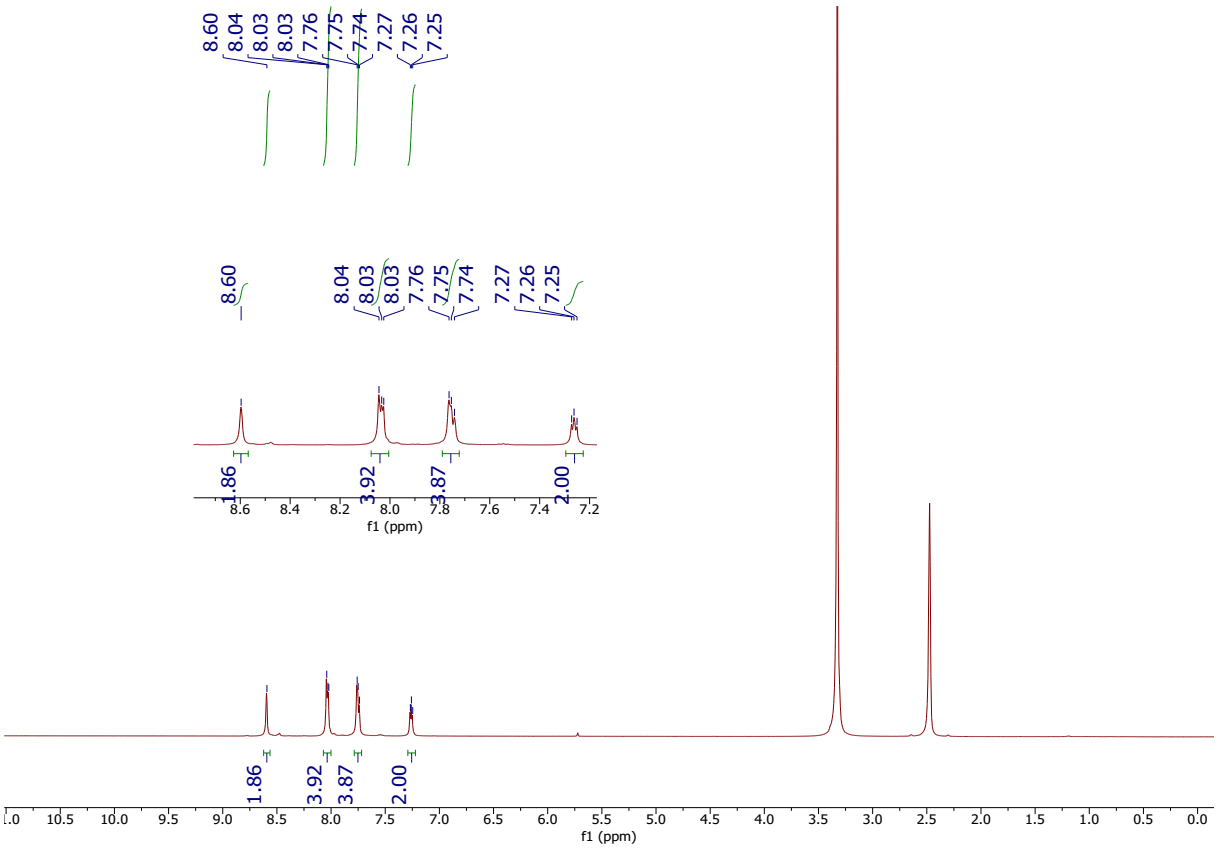

Fig. S5. ^{13}H NMR of **PQ-3DiTP** in DMSO-d_6.

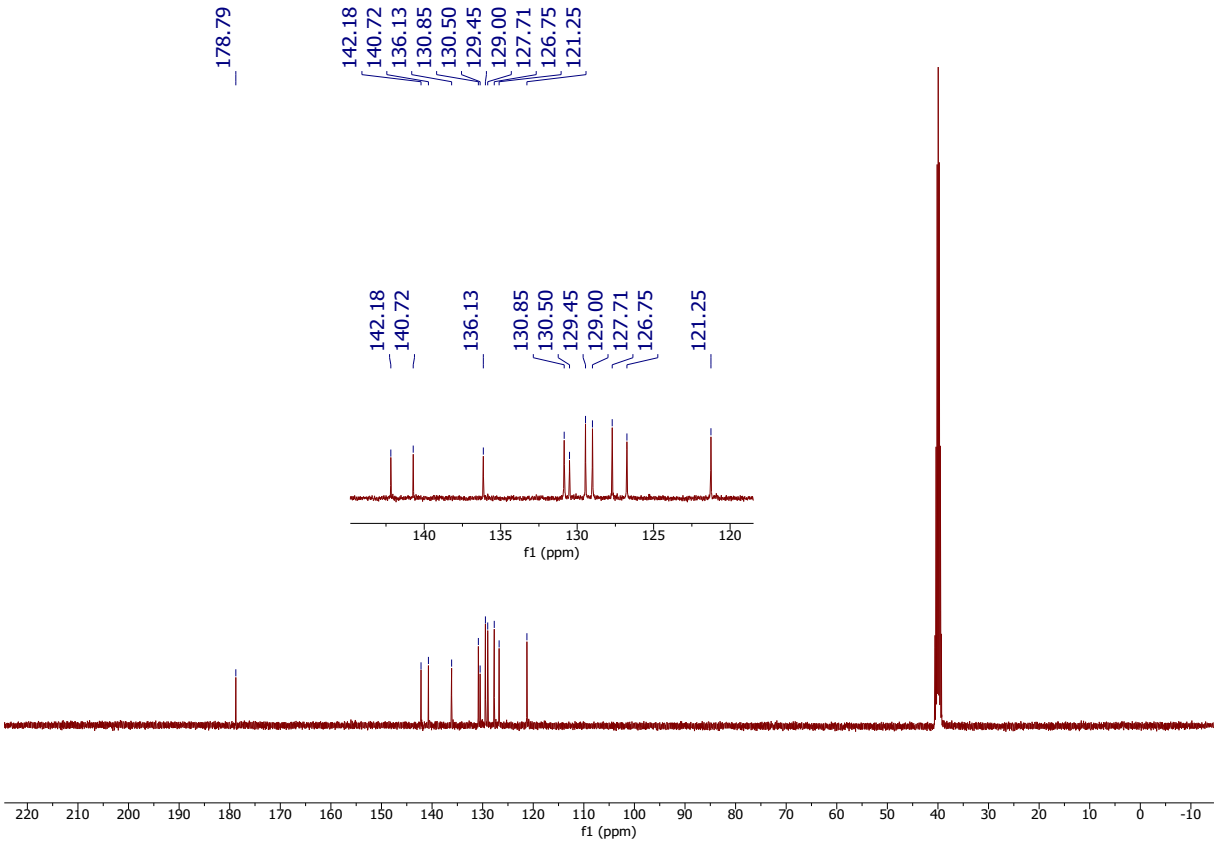

Fig. S6. ^{13}C NMR of **PQ-3DiTP** in DMSO-d_6.

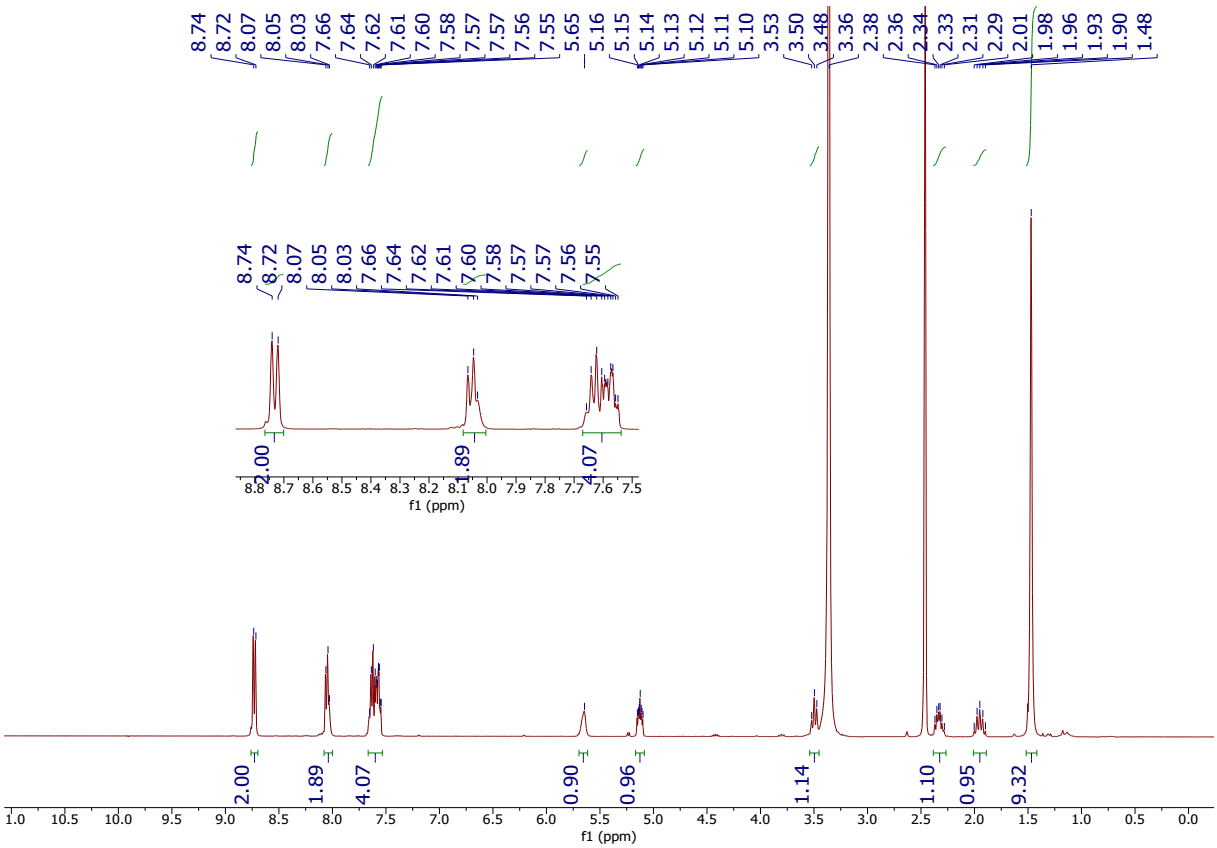

Fig. S7. ^{1}H NMR of **PQ-PY** in DMSO-d_6.

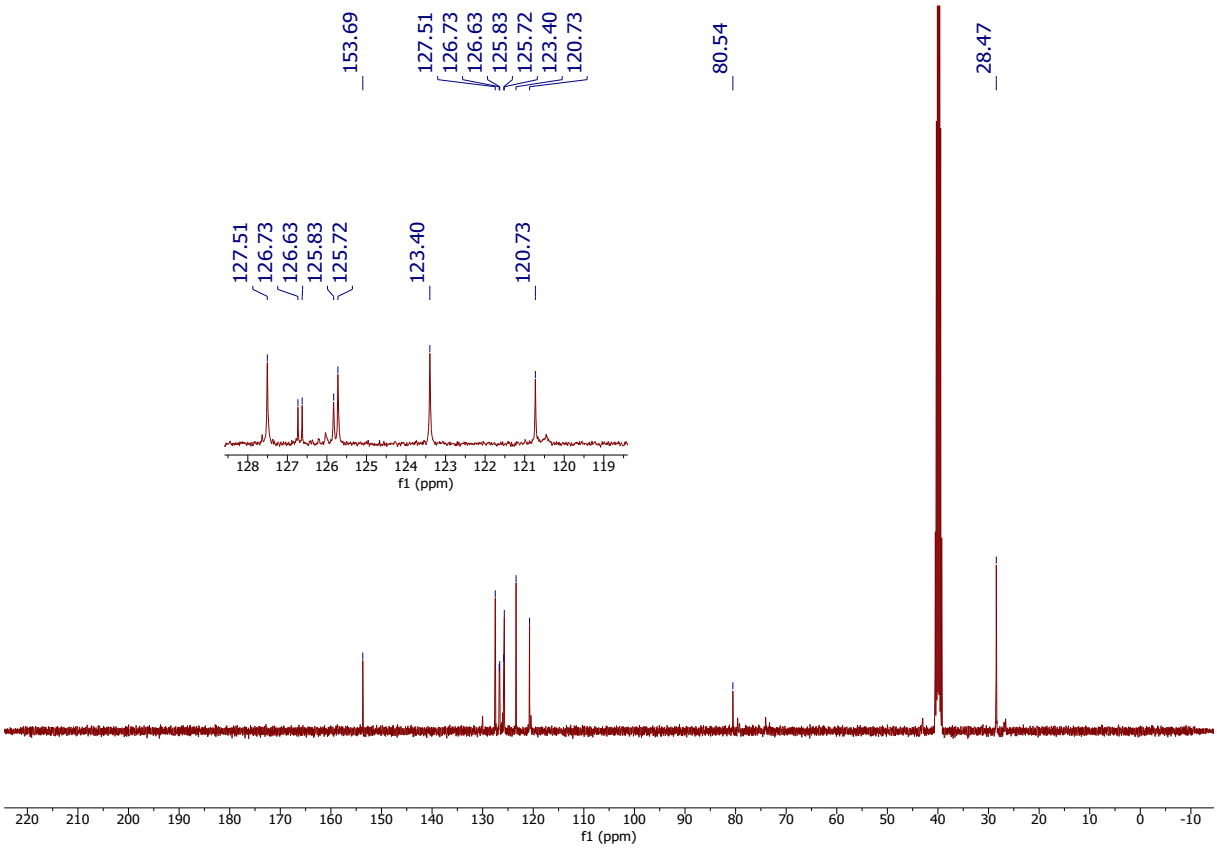

Fig. S8. ^{13}C NMR of **PQ-PY** in DMSO-d_6.

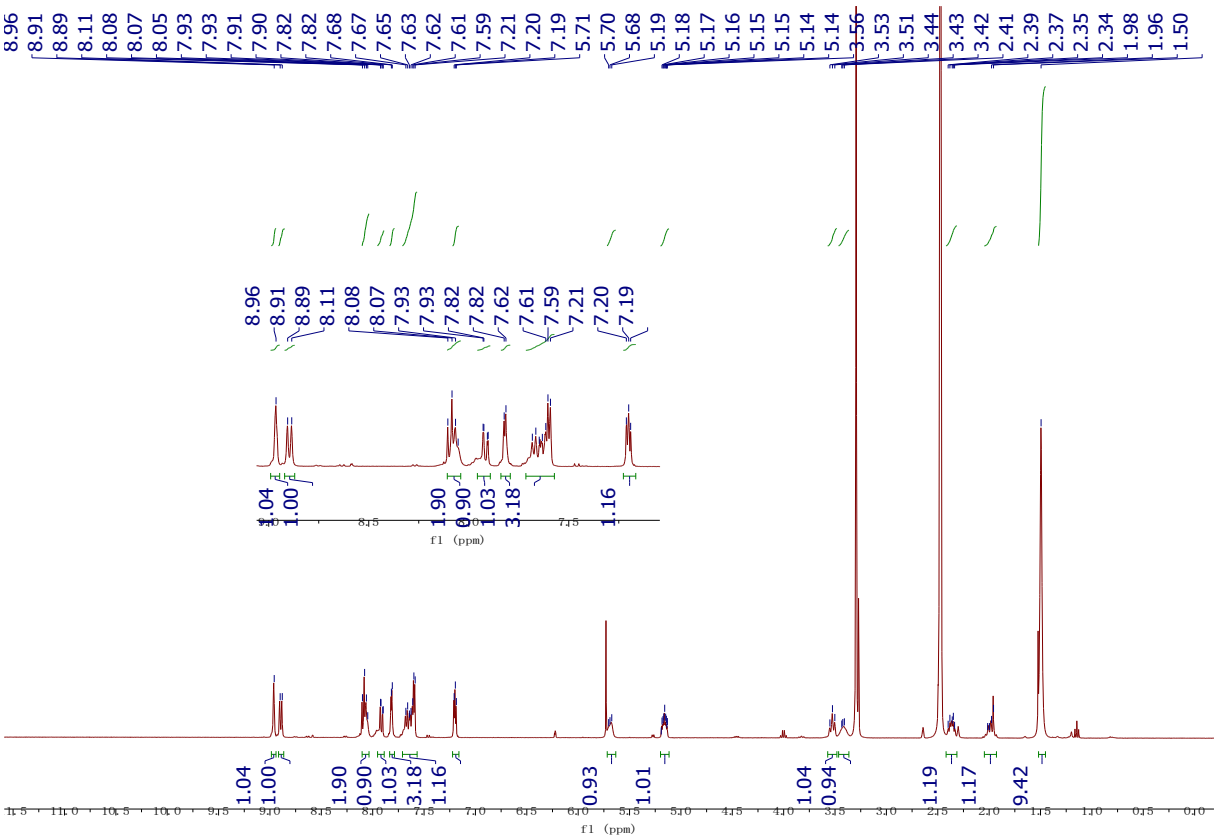

Fig. S9. ^{1}H NMR of **PQ-3TP-PY** in DMSO-*d*$_6$.

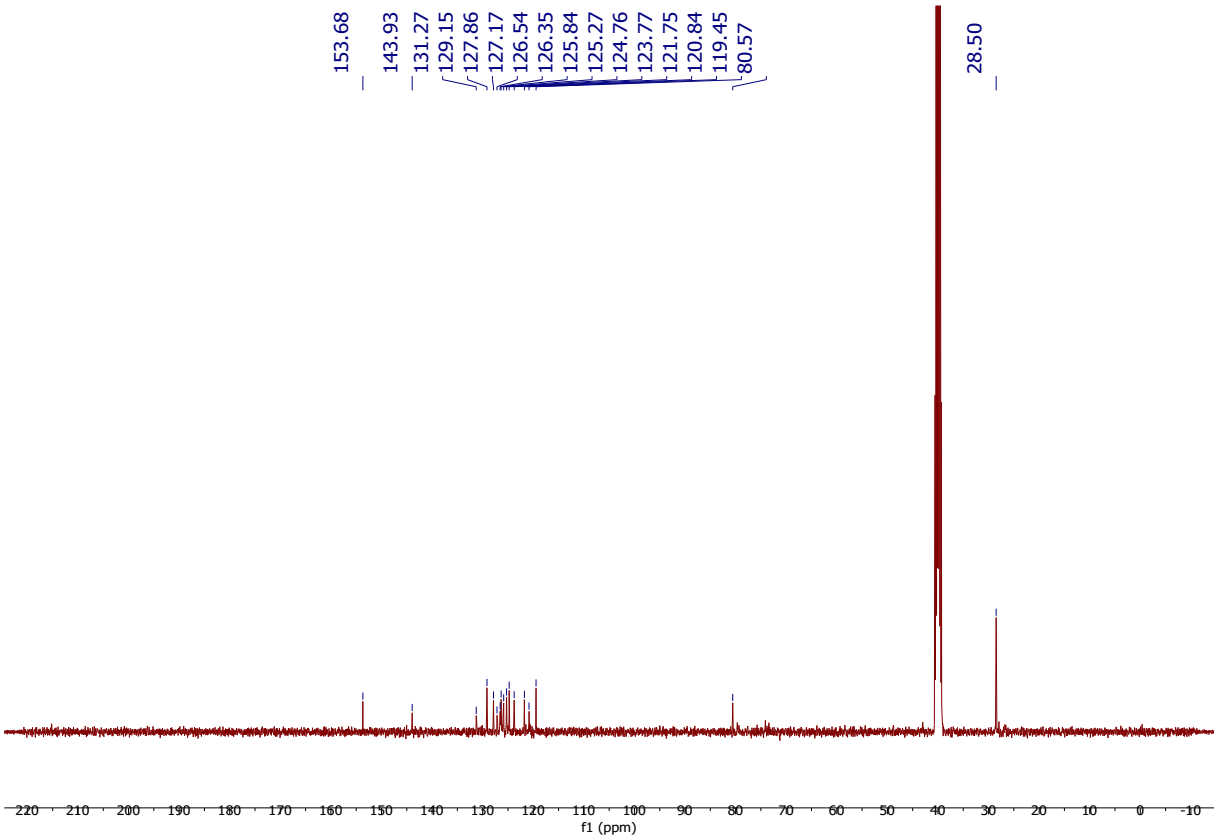

Fig. S10. ^{13}C NMR of **PQ-3TP-PY** in DMSO-*d*$_6$.

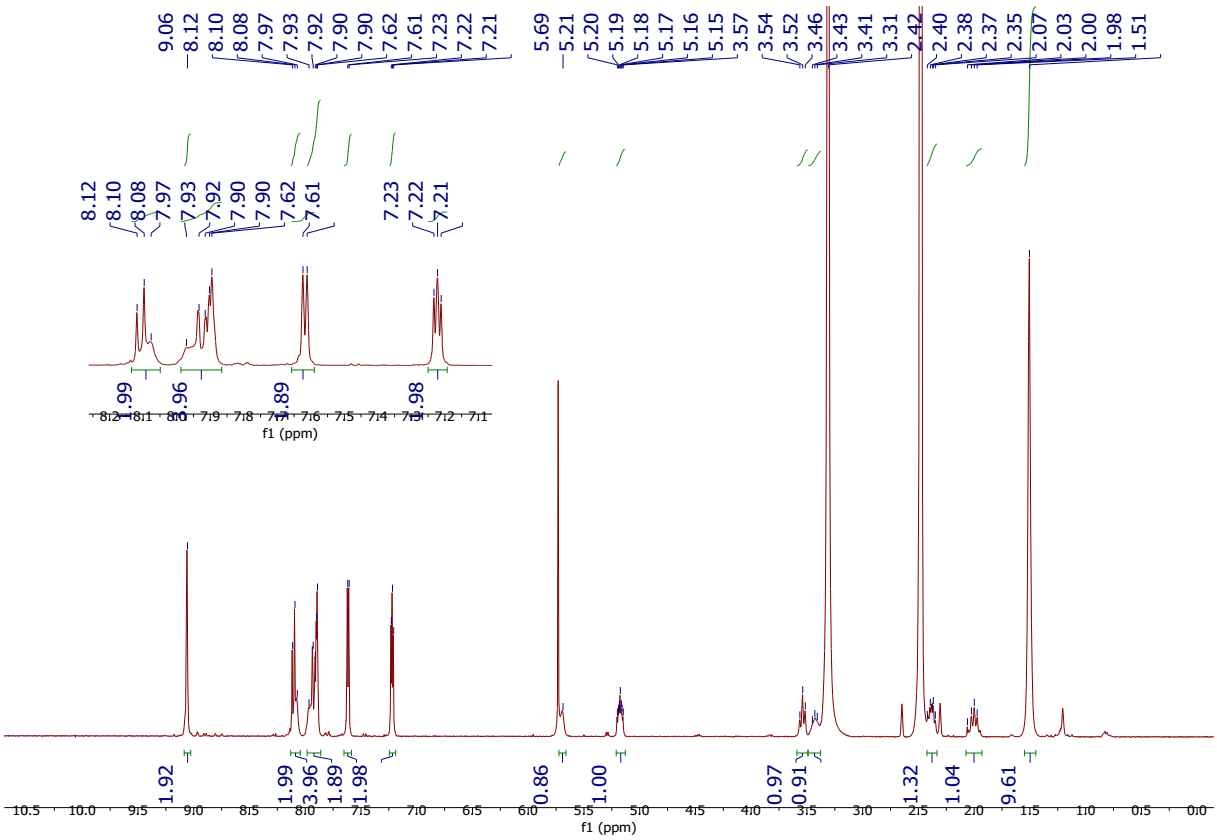

Fig. S11. ^{1}H NMR of **PQ-3DiTP-PY** in DMSO-d_6.

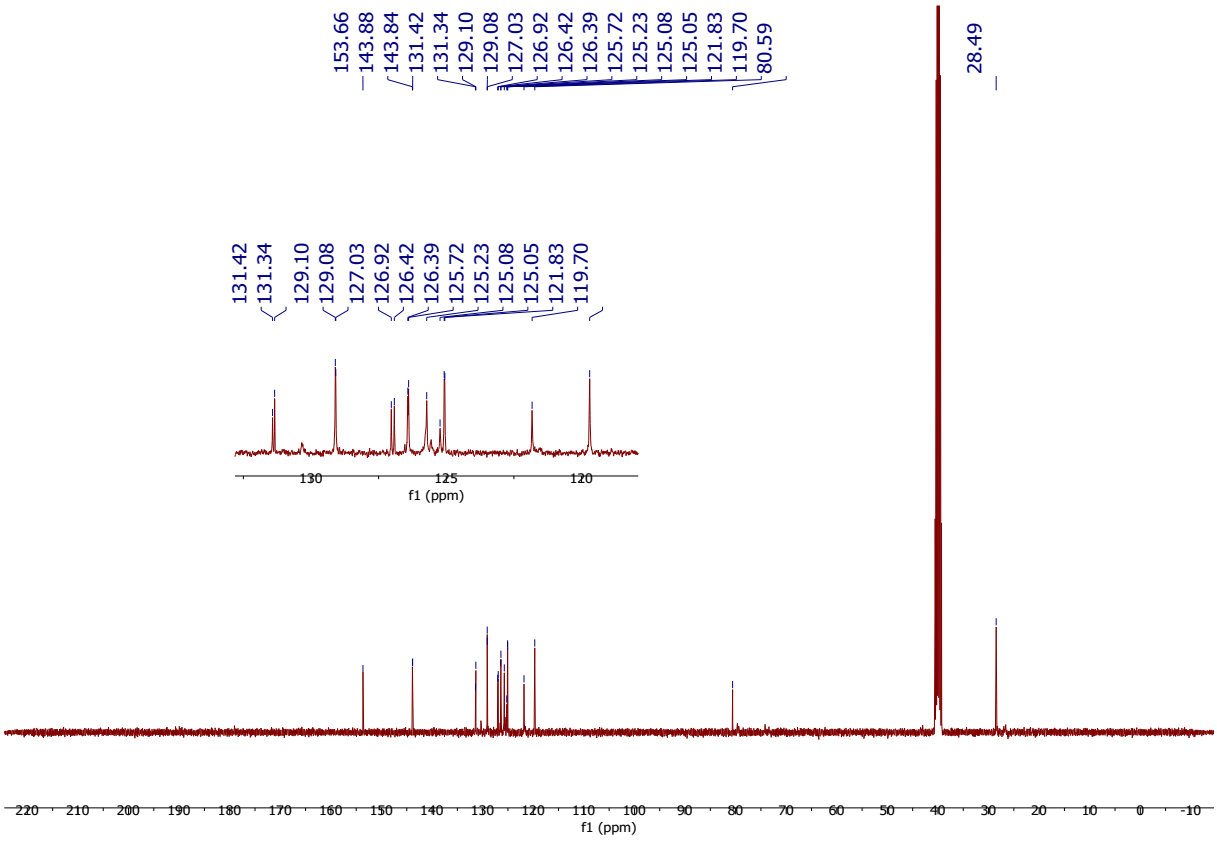

Fig. S12. ^{13}C NMR of **PQ-3DiTP-PY** in DMSO-d_6.

4. Photophysical and Photochemical Studies by UV-Vis Spectroscopy and Transient Absorption Spectroscopy

4.1. UV-Vis Spectra

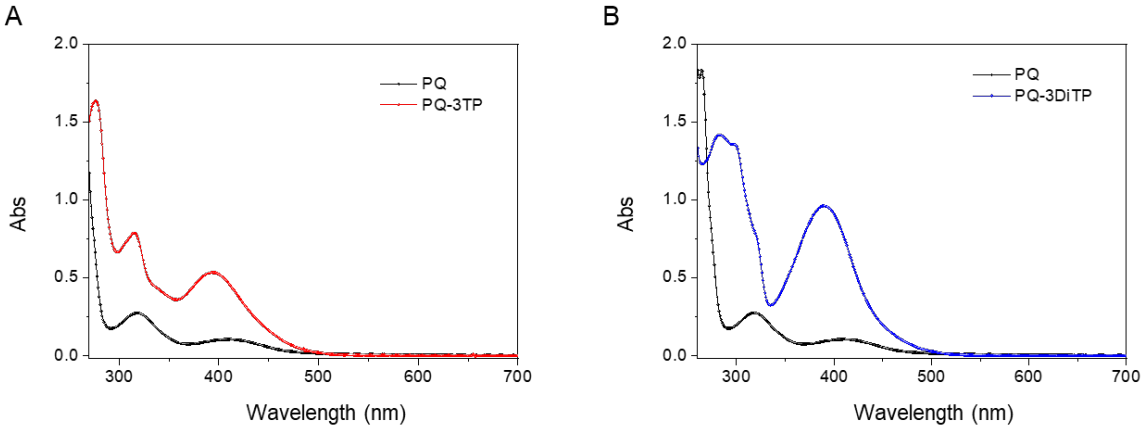

Fig. S13. Comparison of UV-Vis absorption spectra of **PQ** with A) **PQ-3TP**, B) **PQ-3DiTP**. All measurements were performed in MeCN with 50 µM of **PQ**s at 20 °C.

4.2. Analysis of reactions rates

To assess the different reaction rates of the photo-induced [4+2] cycloaddition of the various phenanthrenequinone (**PQ**s) substrates **PY**, we adapted procedures previously published for the evaluation of the kinetics of chemical[10] and photochemical click reactions.[11] Photochemical transformations are strongly dependent on the used light source and setup, *etc.*, as shown *e.g.* for photocatalyic transformations[12] and photoclick reactions.[13,14] Therefore, we determined the respective rate constants *via* UV-Vis absorption spectroscopy using the fixed LED setup, described above, to achieve reliable comparability of the individual substrates. All reactions were performed at the same concentration (**PQ**s: 50 µM, traps: 500 µM) and under irradiation with the same light source and intensity, independently from the molar attenuation coefficient of the respective **PQ**s at this wavelength. Both the wavelength of irradiation (λ_{exc}=390 nm) and λ_{obs} were chosen in the spectral regions where only the starting materials, **PQ**, and the photoclick product, absorb. Rate constants k_{obs} for the different **PQ**s (50 µM) were measured under *pseudo*-first-order conditions with a 10-fold excess of **PY** in MeCN (N_2 atmosphere) by time-dependent analysis. Mixing the appropriate volume of the prepared stock solutions the

desired final concentration was derived in sample vials, and the mixture was transferred into a 1 cm optical path quartz optical cuvette, degassed by N_2. Signals were read out by monitoring the absorption signal of the **PQ**s. The kinetic traces were recorded using the following instrumental parameters: 1 data point per second over the recorded time range. The data were analyzed using single-exponential fits. All data processing was performed using Origin-pro software.

While this treatment does not lead to the best performance of all systems at the applied irradiation wavelength (due to different molar attenuation coefficient at that wavelength), it does (i) facilitate rapid screening of **PQ**s and (ii) give a good impression of the relative reaction rates between individual **PQ**s-**PY** systems.

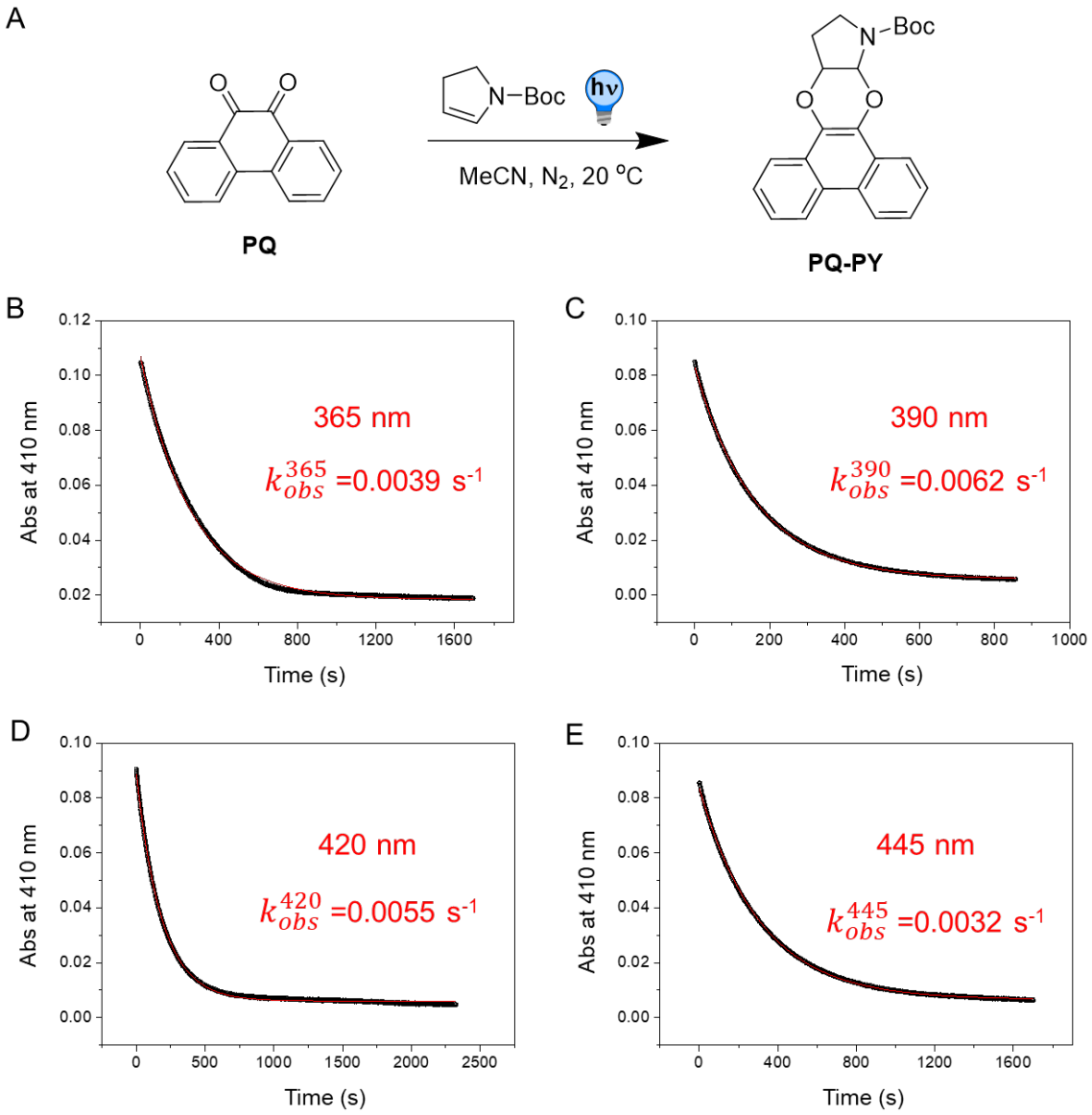

Fig. S14. Photo-induced [4+2] cycloaddition of **PQ** with **PY** upon different light irradiation. Reaction scheme A) and kinetic traces of the photocycloaddition between **PQ** (50 μM) with **PY** (500 μM) in 2.5 mL MeCN (N_2 atmosphere) was irradiated with B) 365 nm, C) 390 nm, D) 420 nm, and E) 445 nm LED at 20 °C. The reaction was monitored by UV-Vis absorption spectra (1 cm cuvette, sample interval 1 s). **PQ-PY** formation was fitted to an exponential rise to the maximum equation, $y = (y_0\text{-}a)\, e^{kobs*t} + b$, to give k_{obs}.

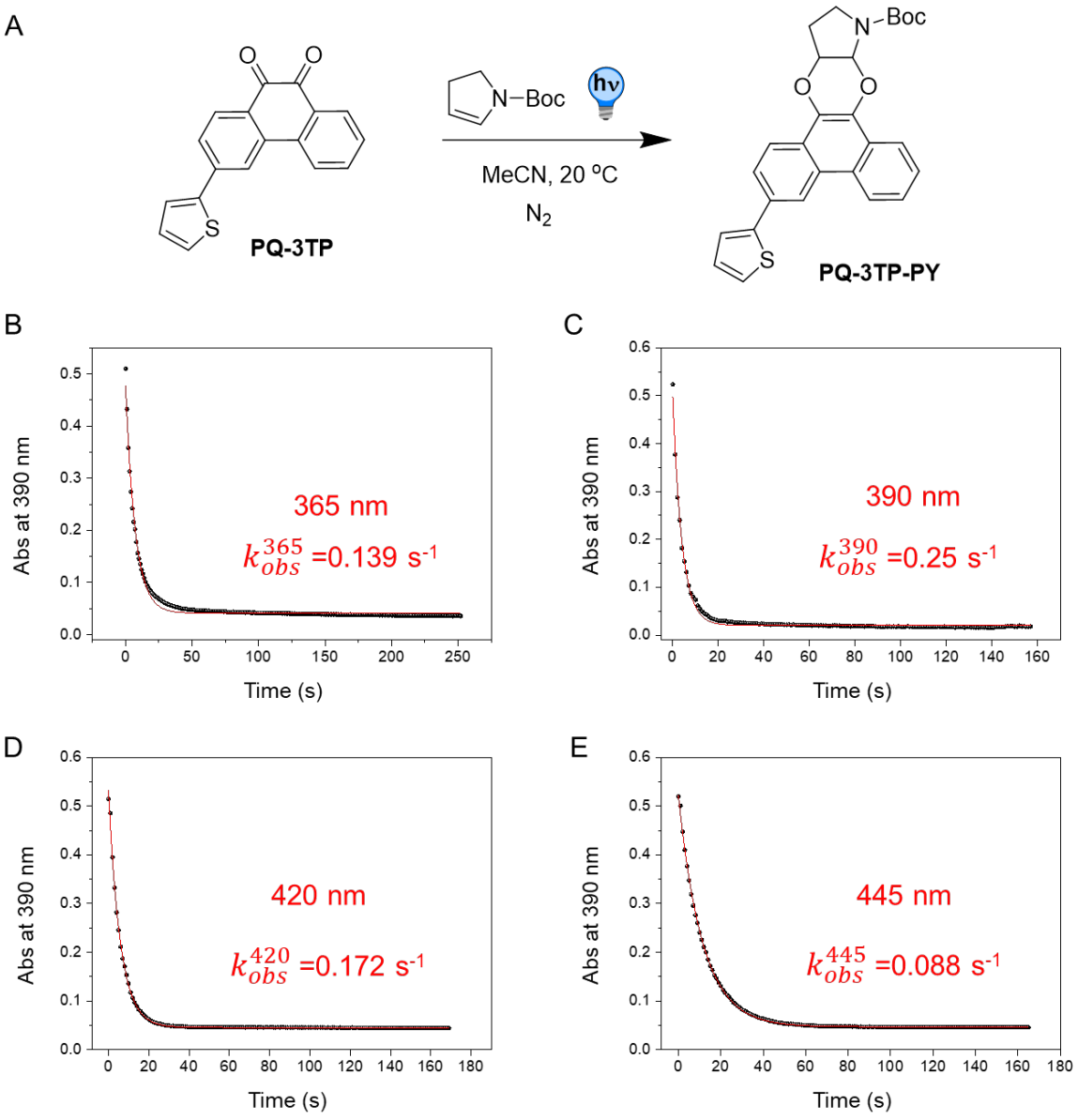

Fig. S15. Photo-induced [4+2] cycloaddition of **PQ-3TP** with **PY** upon different light irradiation. Reaction scheme A) and kinetic traces of the photocycloaddition between **PQ-3TP** (50 μM) with **PY** (500 μM) in 2.5 mL MeCN (N_2 atmosphere) was irradiated with B) 365 nm, C) 390 nm, D) 420 nm, and E) 445 nm LED at 20 °C. The reaction was monitored by UV-Vis absorption spectra (1 cm cuvette, sample interval 1 s). **PQ-3TP-PY** formation was fitted to an exponential rise to the maximum equation, $y = (y_0\text{-}a)\, e^{kobs*t} + b$, to give k_{obs}.

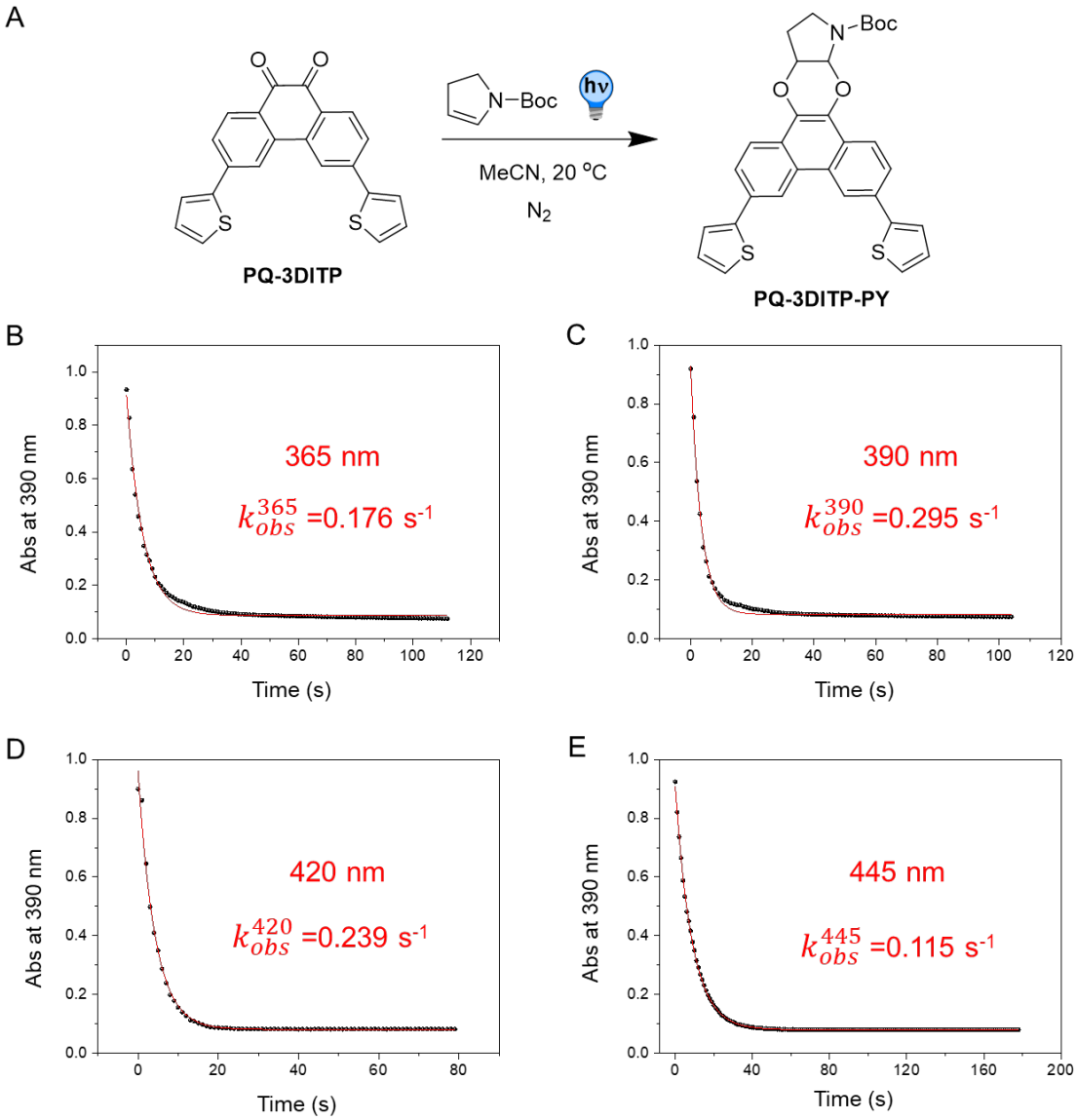

Fig. S16. Photo-induced [4+2] cycloaddition of **PQ-3DiTP** with **PY** upon different light irradiation. Reaction scheme A) and kinetic traces of the photocycloaddition between **PQ-3DiTP** (50 μM) with **PY** (500 μM) in 2.5 mL MeCN (N_2 atmosphere) was irradiated with B) 365 nm, C) 390 nm, D) 420 nm, and E) 445 nm LED at 20 °C. The reaction was monitored by UV-Vis absorption spectra (1 cm cuvette, sample interval 1 s). **PQ-3DiTP-PY** formation was fitted to an exponential rise to the maximum equation, $y = (y_0\text{-}a)\, e^{kobs*t} + b$, to give k_{obs}.

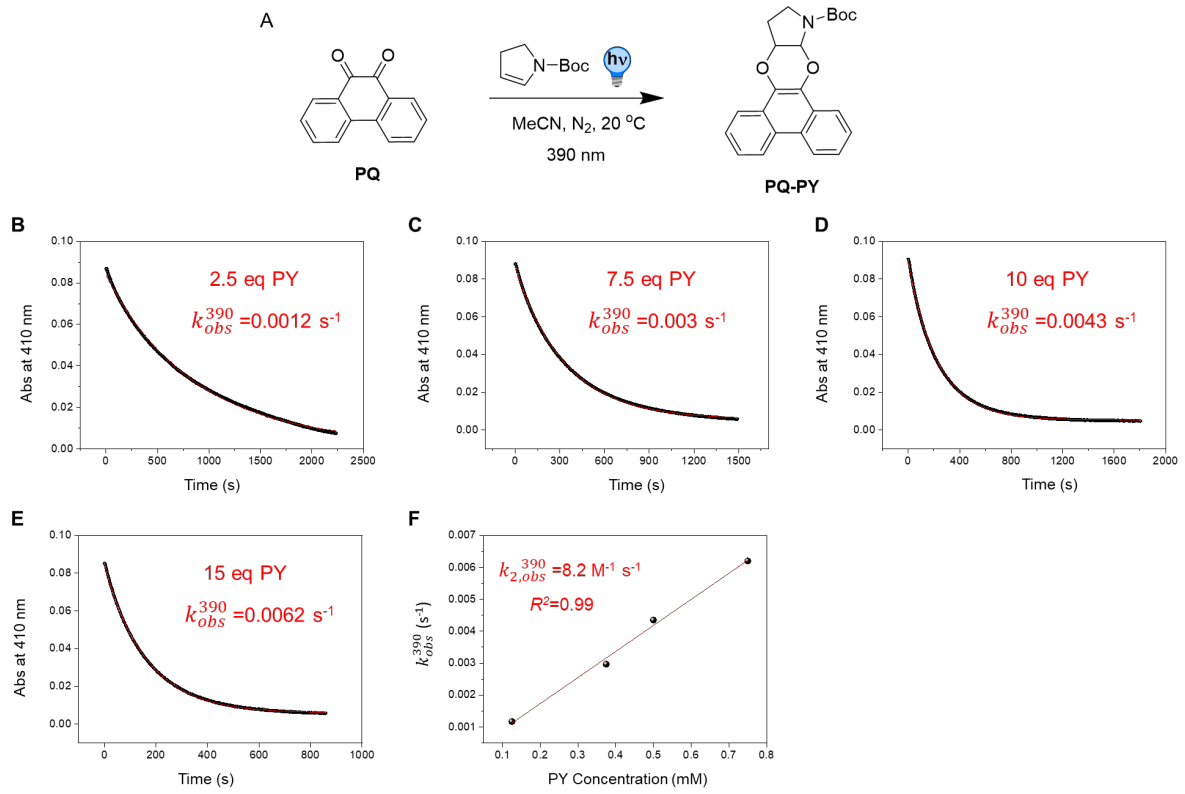

Fig. S17. Reaction scheme A) and kinetic traces of the photocycloaddition between **PQ** and **PY**. 50 μM **PQ** with different concentrations of **PY** ((B) 0.125 mM, (C) 0.375 mM, (D) 0.5 mM, and (E) 0.75 mM, respectively) in 2.5 mL MeCN (N_2 atmosphere); the reaction mixture was irradiated with 390 nm LED at 20 ºC. The formation of the [4+2] cycloaddition product **PQ-PY** was monitored by UV-Vis absorption spectroscopy (λ_{obs}=410 nm, 1 cm cuvette, sample interval 1 s) and the trace was fitted exponentially using the equation, $y = (y_0\text{-}a)\, e^{kobs*t} + b$, to give k_{obs}^{390}. F) Plot of k_{obs}^{390} vs **PY** concentration. The second-order rate constant $k_{2,obs}^{390}$ was determined to be 8.2 M^{-1} s^{-1} based on the slope of the fitted line.

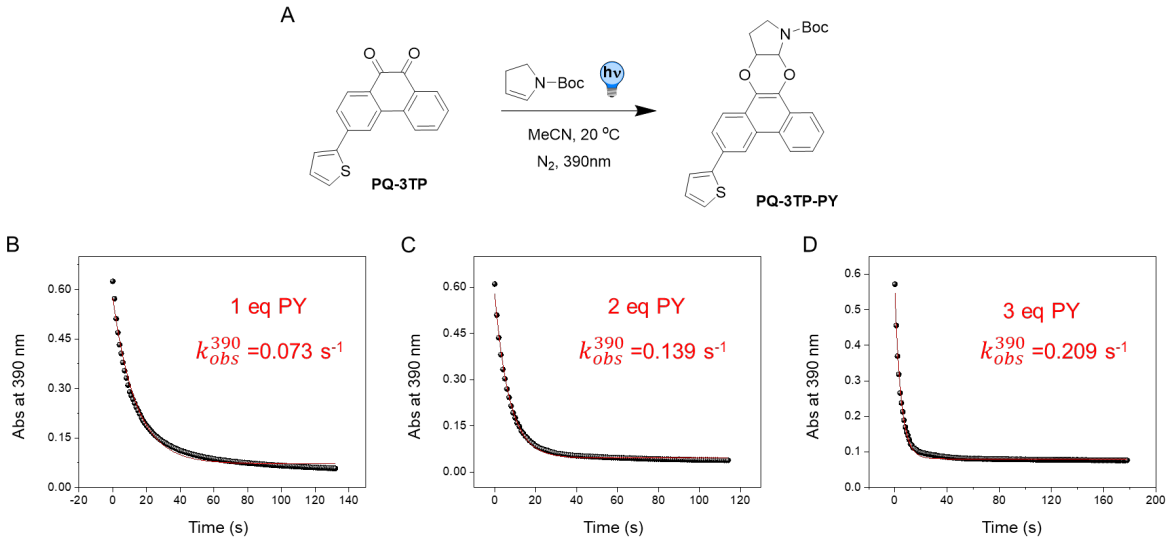

Fig. S18. Reaction scheme A) and kinetic traces of the photocycloaddition between **PQ-3TP** and **PY**. 50 µM **PQ-3TP** with different concentrations of **PY** ((B) 0.05 mM, (C) 0.1 mM, and (D) 0.15 mM, respectively) in 2.5 mL MeCN (N_2 atmosphere); the reaction mixture was irradiated with 390 nm LED at 20 °C. The formation of the [4+2] cycloaddition product **PQ-3TP-PY** was monitored by UV-Vis absorption spectroscopy (λ_{obs}=390 nm, 1 cm cuvette, sample interval 1 s) and the trace was fitted exponentially using the equation, $y = (y_0\text{-}a)\, e^{kobs*t} + b$, to give k_{obs}^{390}.

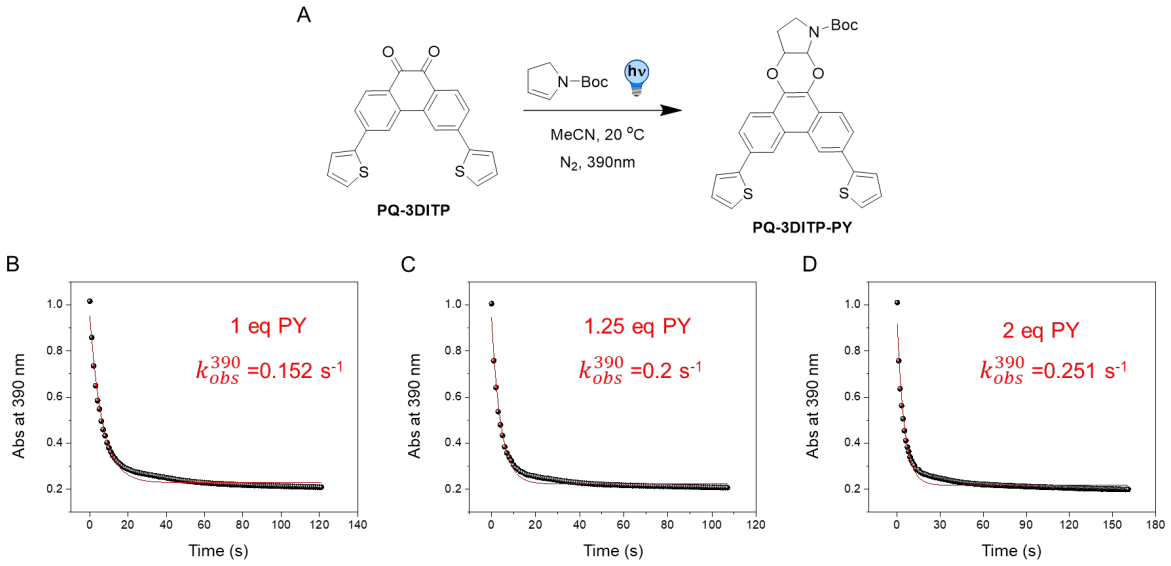

Fig. S19. Reaction scheme A) and kinetic traces of the photocycloaddition between **PQ-3DiTP** and **PY**. 50 µM **PQ-3DiTP** with different concentrations of **PY** ((B) 0.05 mM, (C) 0.0625 mM, and (D) 0.1 mM, respectively) in 2.5 mL MeCN (N_2 atmosphere); the reaction mixture was irradiated with 390 nm LED at 20 °C. The formation of the [4+2] cycloaddition product **PQ-3DiTP-PY** was monitored by UV-Vis absorption spectroscopy (λ_{obs}=390 nm, 1 cm cuvette, sample interval 1 s) and the trace was fitted exponentially using the equation, $y = (y_0\text{-}a)\, e^{kobs*t} + b$, to give k_{obs}^{390}.

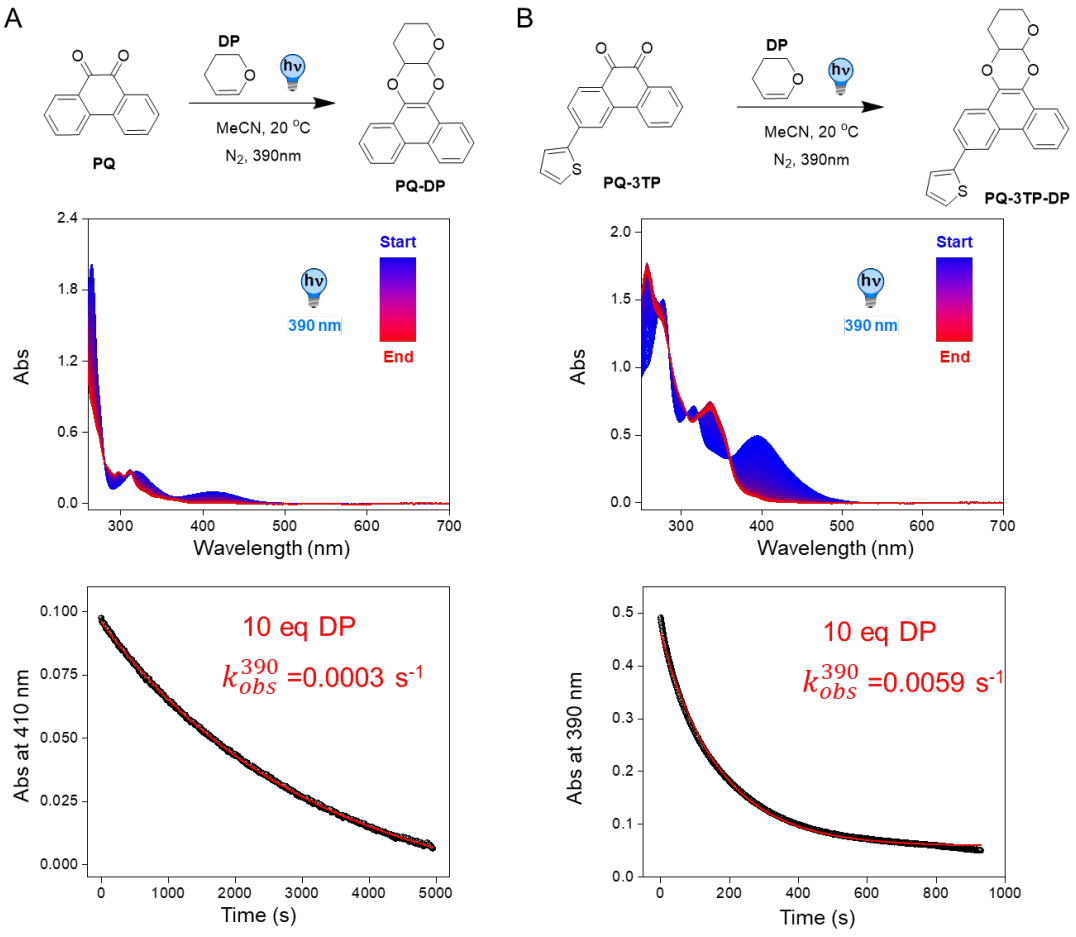

Figure S20. Photo-induced [4+2] cycloaddition of **A) PQ** and **B) PQ-3TP** with **DP** upon 390 nm light irradiation. Reaction scheme and kinetic traces of the photocycloaddition between **PQ**s (50 µM) with **DP** (500 µM) in 2.5 mL MeCN (N_2 atmosphere) was irradiated with 390 nm LED at 20 °C. The reaction was monitored by UV-Vis absorption spectra (1 cm cuvette, sample

interval 1 s). **PQs-DP** formation was fitted to an exponential rise to the maximum equation, y = (y_0-a) e ^{kobs*t} + b, to give k_{obs}.

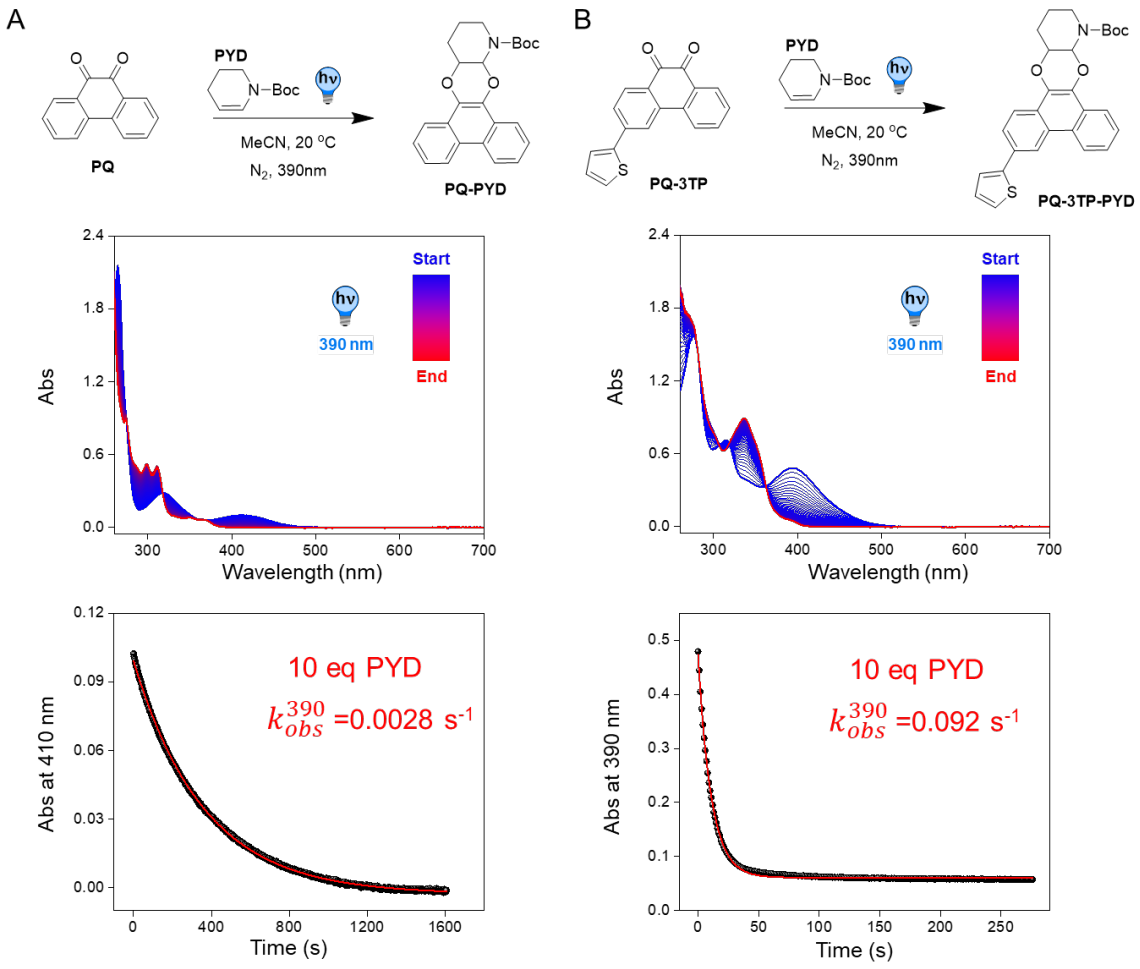

Figure S21. Photo-induced [4+2] cycloaddition of **A) PQ** and **B) PQ-3TP** with **PYD** upon 390 nm light irradiation. Reaction scheme and kinetic traces of the photocycloaddition between **PQ**s (50 μM) with **PYD** (500 μM) in 2.5 mL MeCN (N_2 atmosphere) was irradiated with 390 nm LED at 20 °C. The reaction was monitored by UV-Vis absorption spectra (1 cm cuvette, sample interval 1 s). **PQs-PYD** formation was fitted to an exponential rise to the maximum equation, y = (y_0-a) e ^{kobs*t} + b, to give k_{obs}.

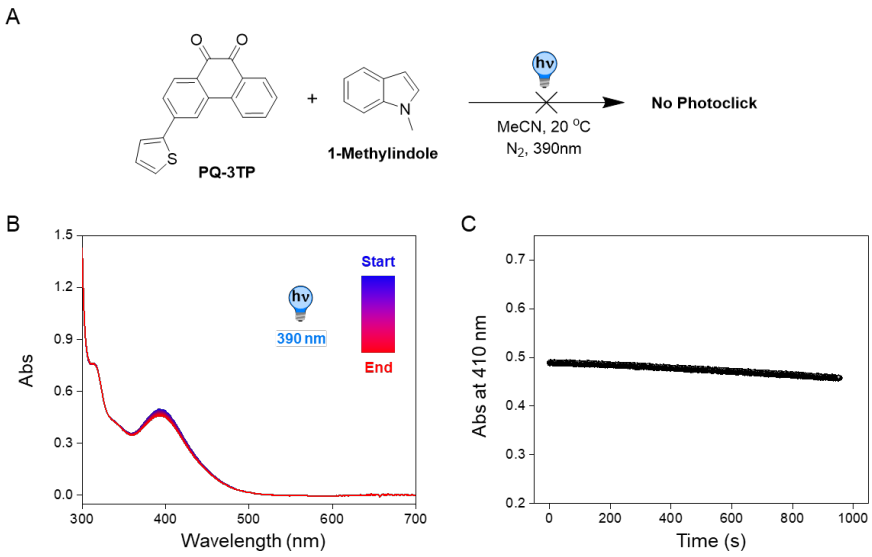

Figure S22. Time-resolved UV-Vis absorption spectra of **PQ-3TP**/**1-Methylindole** (50 μM/500 μM, N_2 atmosphere) under 390 nm light irradiation over 15 min. The measurement was performed at 20 °C, sample interval 1 s.

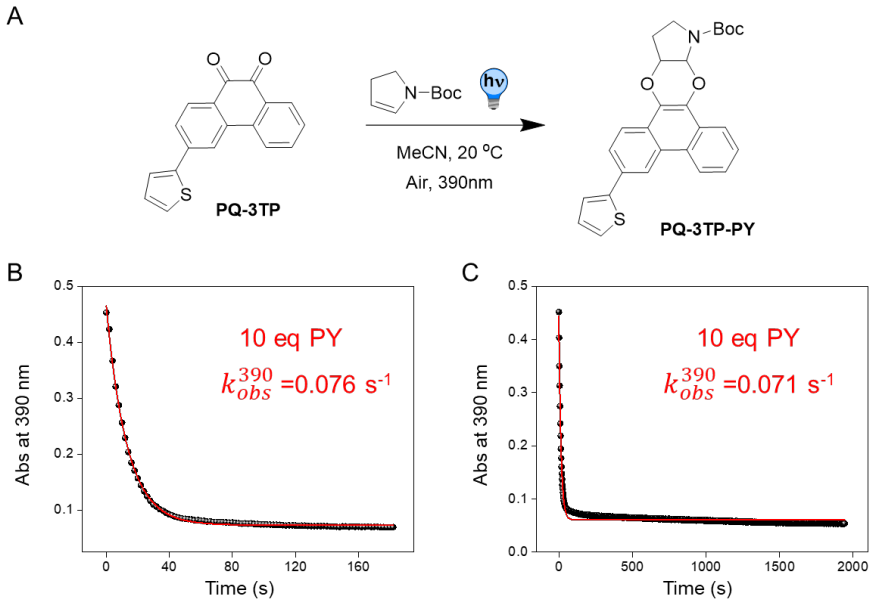

Figure S23. Reaction scheme **A)** and kinetic traces of the photocycloaddition between **PQ-3TP** and **PY** with **B)** short (3 min) and **C)** long time (30 min) irradiation. 50 μM **PQ-3TP** with 500 μM **PY** in 2.5 mL MeCN (air atmosphere); the reaction mixture was irradiated with 390 nm LED at 20 °C. The formation of the [4+2] cycloaddition product **PQ-3TP-PY** was monitored

by UV-Vis absorption spectroscopy (λ_{obs} = 390 nm, 1 cm cuvette, sample interval 2 s) and the trace was fitted exponentially using the equation, y = (y_0-a) e ^{kobs*t} + b, to give k_{obs}^{390}.

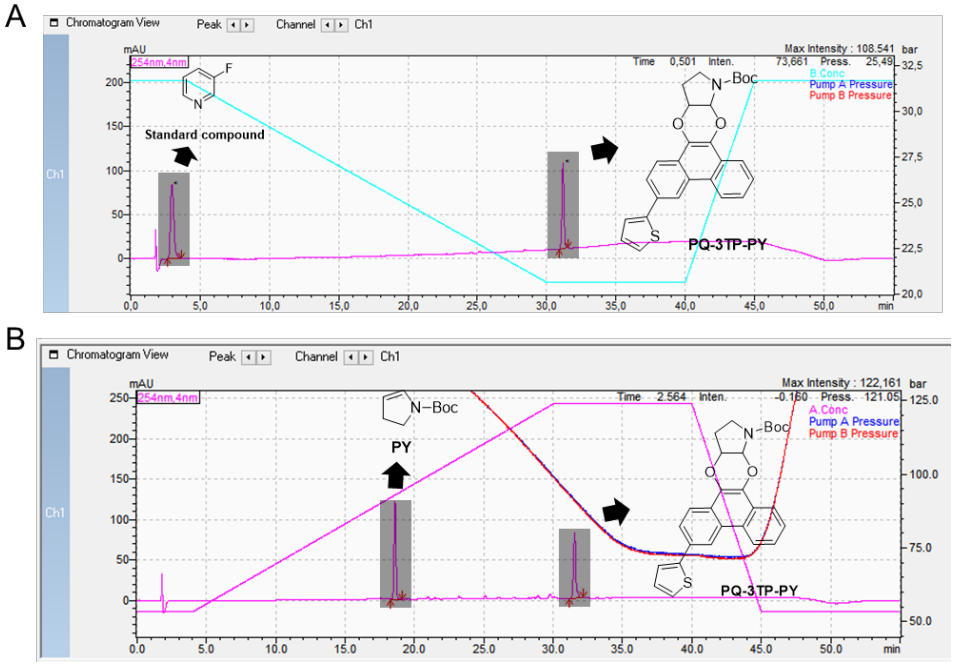

Figure S24. HPLC trace of **A) PQ-3TP-PY** and **B)** the reaction mixture (**PQ-3TP_PY**) after 30 min irradiation with 390 nm LED in air.

4.3. Photoclick reaction quantum yields

UV/Vis evolution spectra were recorded using the setup described above with the 390B LED. The photon flux was determined using standard ferrioxalate actinometry, which provided a value of 3.94052×10^{-5} mol photons s^{-1} for the 390B LED.[15] Spectra were collected over 10000 seconds, exported, and processed in SpectraGryph and OriginPro. Baseline corrections were carried out to correct for baseline drifting, after which the data was processed in QYMain (https://www.nature.com/articles/srep41145#Sec14) developed by Stranius & Börjesson.[16]

$$\frac{d[A]}{dt} = \frac{I * QY_{(A\rightarrow B)} * \beta_A}{N_a * V} + \frac{I * QY_{(B\rightarrow A)} * \beta_B}{N_a * V} + [A] * k_{(B\rightarrow A)}$$

was used to fit the data collected in the first 10% reaction process using the following molar extinction coefficients and absorbance data at the irradiation wavelength (390 nm). Normalized absorbance (λ=460 nm) fitting plot and Φ_P are shown below:

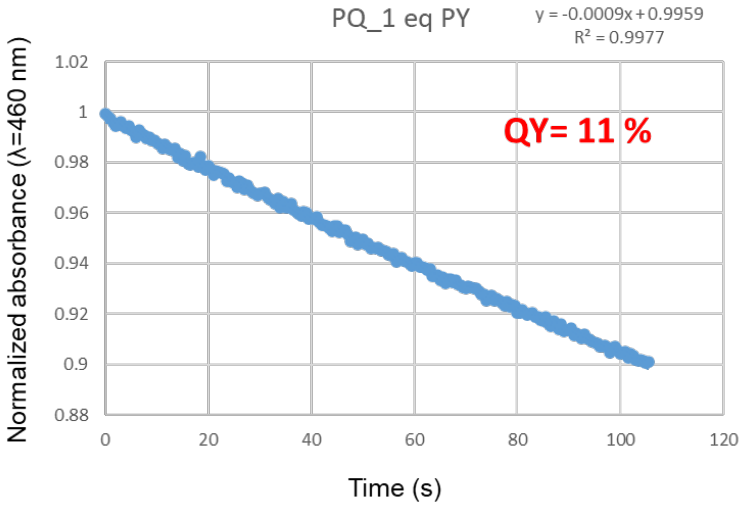

Fig. S25. Photoclick reaction of **PQ** (2 mM) with 1 eq **PY** (2 mM). The measurement was done in a 1 cm quartz cuvette with a 390 nm LED irradiation in N_2 atmosphere at 20 ºC, followed by UV-Vis absorption spectra.

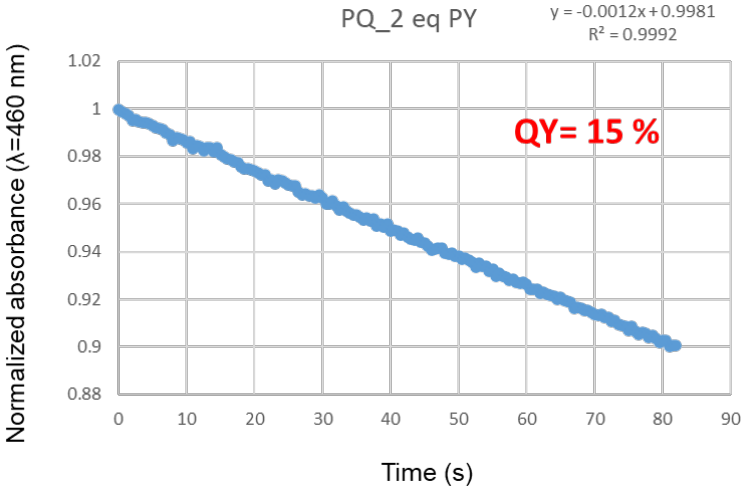

Fig. S26. Photoclick reaction Quantum Yield calculation of **PQ** (2 mM) toward 2 eq **PY** (4 mM). The measurement was done in a 1 cm quartz cuvette with a 390 nm LED irradiation in N_2 atmosphere at 20 ºC, followed by UV-Vis absorption spectra.

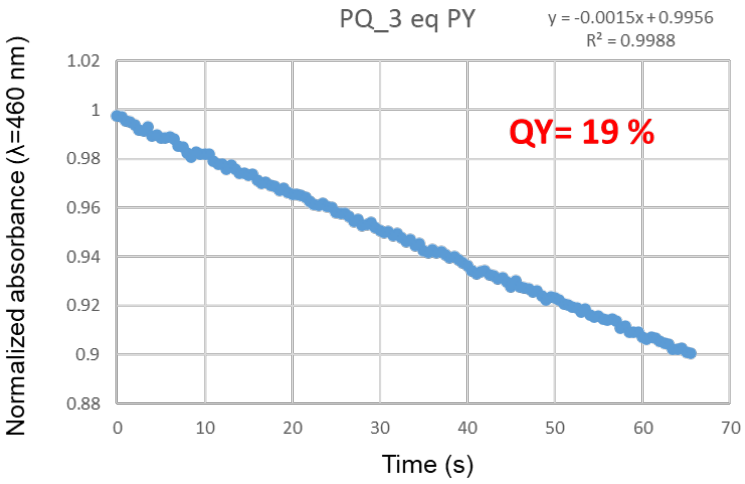

Fig. S27. Photoclick reaction Quantum Yield calculation of **PQ** (2 mM) toward 3 eq **PY** (6 mM). The measurement was done in a 1 cm quartz cuvette with a 390 nm LED irradiation in N_2 atmosphere at 20 ºC, followed by UV-Vis absorption spectra.

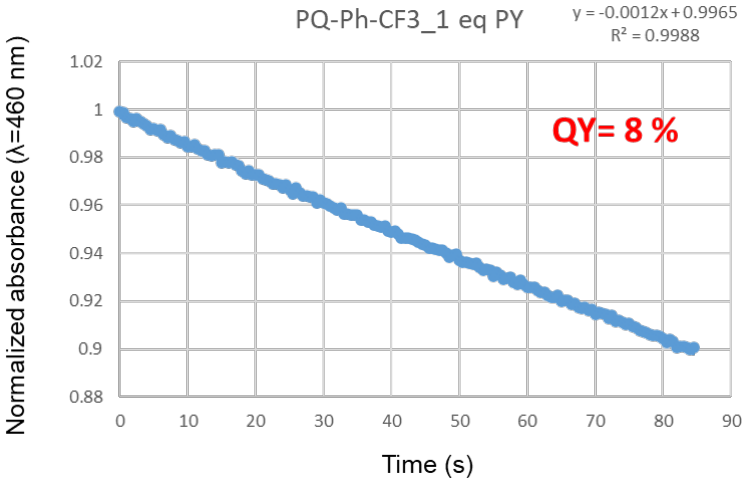

Fig. S28. Photoclick reaction Quantum Yield calculation of **PQ-Ph-CF$_3$** (1 mM) toward 1 eq **PY** (1 mM). The measurement was done in a 1 cm quartz cuvette with a 390 nm LED irradiation in N_2 atmosphere at 20 ºC, followed by UV-Vis absorption spectra.

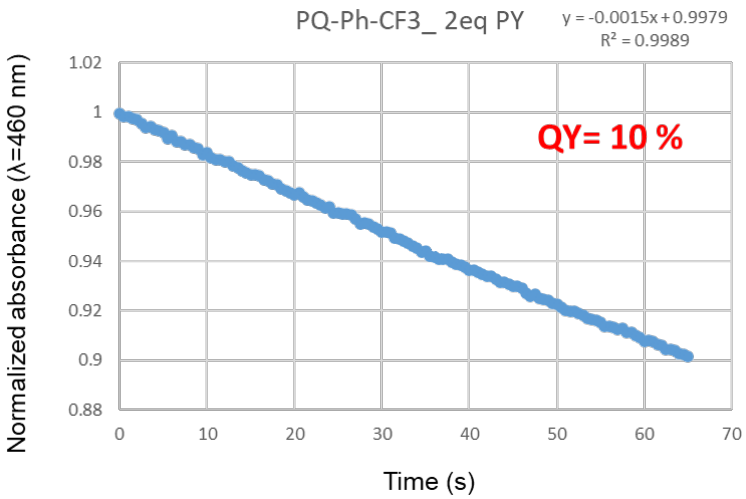

Fig. S29. Photoclick reaction Quantum Yield calculation of **PQ-Ph-CF$_3$** (1 mM) toward 2 eq **PY** (2 mM). The measurement was done in a 1 cm quartz cuvette with a 390 nm LED irradiation in N_2 atmosphere at 20 ºC, followed by UV-Vis absorption spectra.

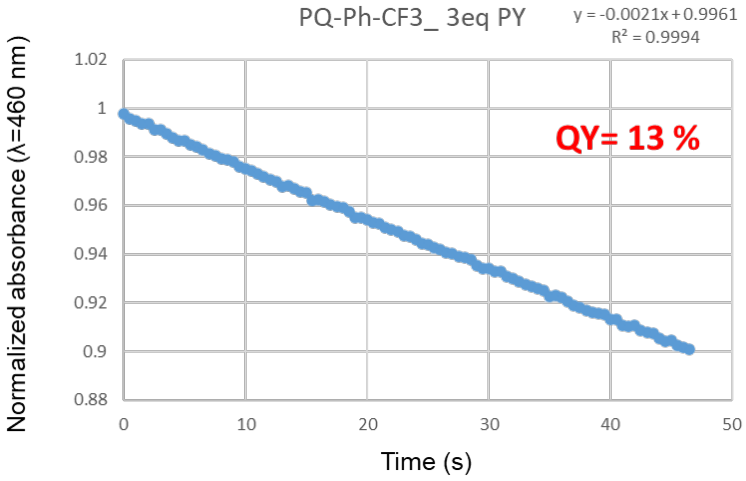

Fig. S30. Photoclick reaction Quantum Yield calculation of **PQ-Ph-CF$_3$** (1 mM) 3 eq **PY** (3 mM). The measurement was done in a 1 cm quartz cuvette with a 390 nm LED irradiation in N_2 atmosphere at 20 ºC, followed by UV-Vis absorption spectra.

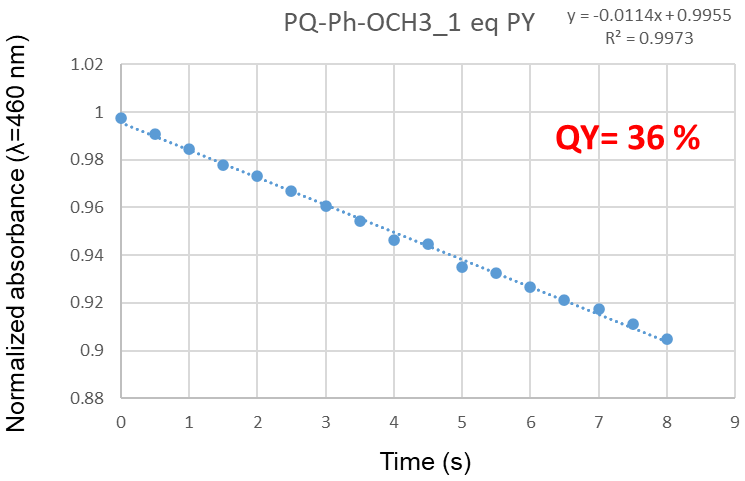

Fig. S31. Photoclick reaction Quantum Yield calculation of **PQ-Ph-OCH$_3$** (0.5 mM) toward 1 eq **PY** (0.5 mM). The measurement was done in a 1 cm quartz cuvette with a 390 nm LED irradiation in N_2 atmosphere at 20 ºC, followed by UV-Vis absorption spectra.

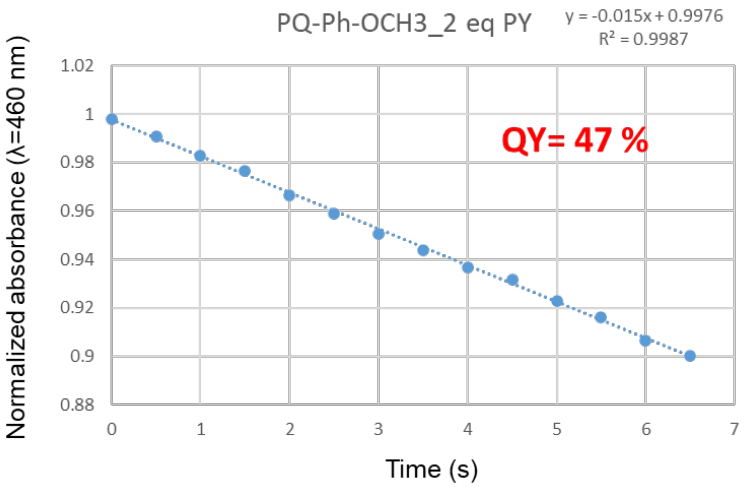

Fig. S32. Photoclick reaction Quantum Yield calculation of **PQ-Ph-OCH$_3$** (0.5 mM) toward 2 eq **PY** (1 mM). The measurement was done in a 1 cm quartz cuvette with a 390 nm LED irradiation in N_2 atmosphere at 20 ºC, followed by UV-Vis absorption spectra.

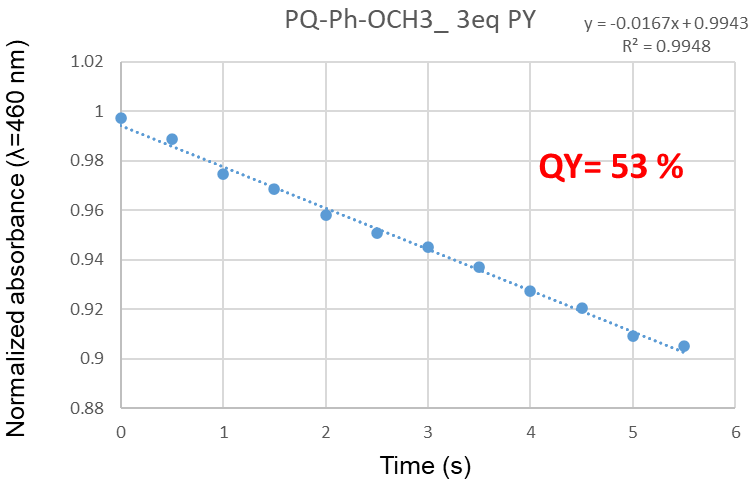

Fig. S33. Photoclick reaction Quantum Yield calculation of **PQ-Ph-OCH$_3$** (0.5 mM) toward 3 eq **PY** (1.5 mM). The measurement was done in a 1 cm quartz cuvette with a 390 nm LED irradiation in N_2 atmosphere at 20 ºC, followed by UV-Vis absorption spectra.

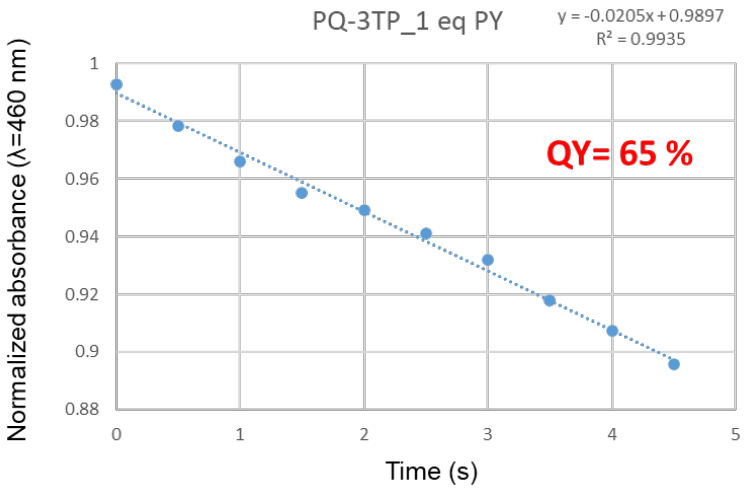

Fig. S34. Photoclick reaction Quantum Yield calculation of **PQ-3TP** (0.5 mM) toward 1 eq **PY** (0.5 mM). The measurement was done in a 1 cm quartz cuvette with a 390 nm LED irradiation in N_2 atmosphere at 20 ºC, followed by UV-Vis absorption spectra.

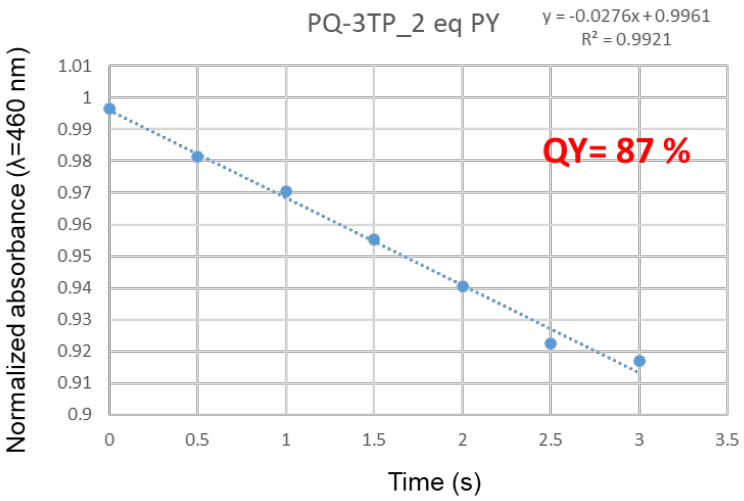

Fig. S35. Photoclick reaction Quantum Yield calculation of **PQ-3TP** (0.5 mM) toward 2 eq **PY** (1 mM). The measurement was done in a 1 cm quartz cuvette with a 390 nm LED irradiation in N_2 atmosphere at 20 ºC, followed by UV-Vis absorption spectra.

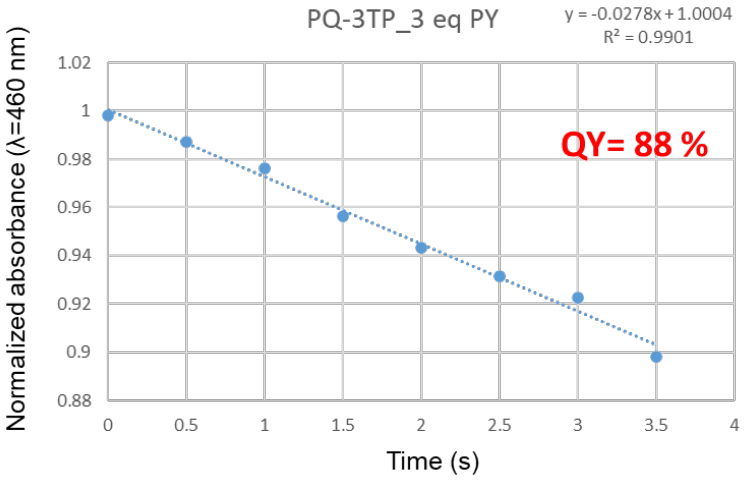

Fig. S36. Photoclick reaction Quantum Yield calculation of **PQ-3TP** (0.5 mM) toward 3 eq **PY** (1.5 mM). The measurement was done in a 1 cm quartz cuvette with a 390 nm LED irradiation in N_2 atmosphere at 20 ºC, followed by UV-Vis absorption spectra.

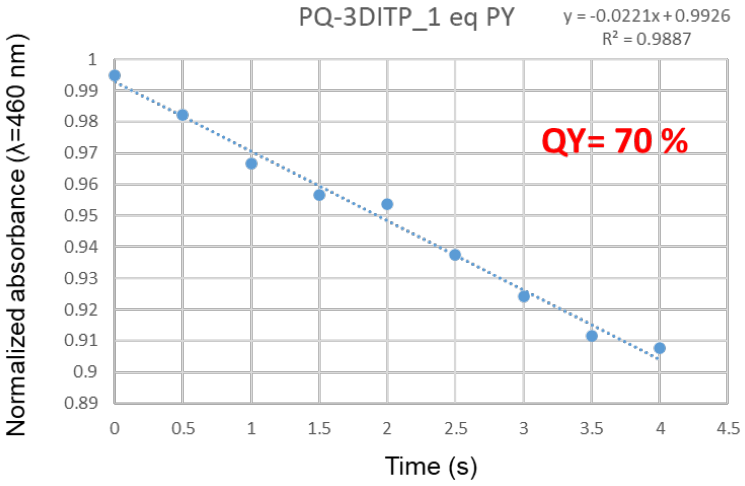

Fig. S37. Photoclick reaction Quantum Yield calculation of **PQ-3DiTP** (0.5 mM) toward 10 eq **PY** (0.5 mM). The measurement was done in a 1 cm quartz cuvette with a 390 nm LED irradiation in N_2 atmosphere at 20 ºC, followed by UV-Vis absorption spectra.

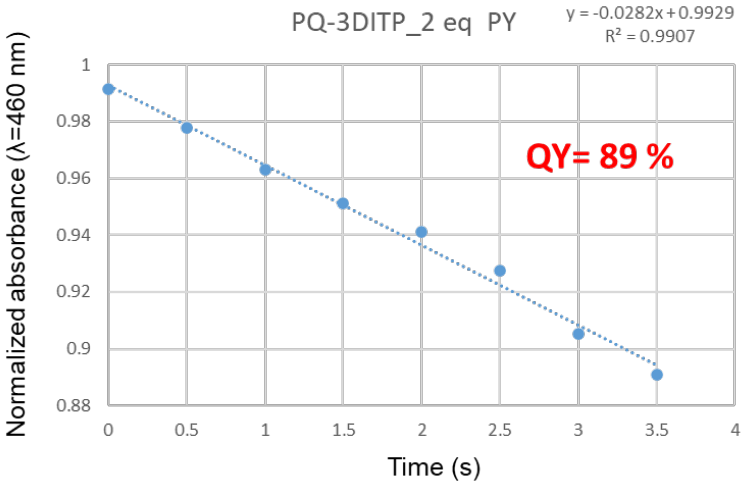

Fig. S38. Photoclick reaction Quantum Yield calculation of **PQ-3DiTP** (0.5 mM) toward 2 eq **PY** (1 mM). The measurement was done in a 1 cm quartz cuvette with a 390 nm LED irradiation in N_2 atmosphere at 20 ºC, followed by UV-Vis absorption spectra.

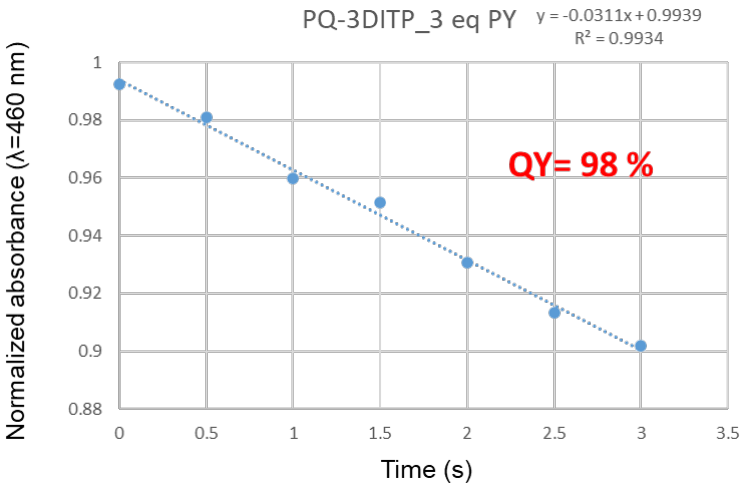

Fig. S39. Photoclick reaction Quantum Yield calculation of **PQ-3DiTP** (0.5 mM) toward 10 eq **PY** (1.5 mM). The measurement was done in a 1 cm quartz cuvette with a 390 nm LED irradiation in N_2 atmosphere at 20 °C, followed by UV-Vis absorption spectra.

4.4. Femtosecond Transient Absorption Spectroscopy

Transient absorption spectroscopy was applied to determine the rate of triplet state formation in **PQ** and its derivatives. The molecules **PQ**, **PQ-3TP** and **PQ-3DiTP** were tested in MeCN, with the excitation wavelength set at 400 nm. All the data were analyzed using a global fit procedure and employing a sequential linear decay kinetic scheme, obtaining the EADS (Evolution Associated Difference Spectra) and the rate constants describing the excited state dynamics.

The EADS obtained analyzing the transient spectra of **PQ** are reported in Figure S40. Soon after excitation the transient spectrum presents a broad excited state absorption band (ESA) peaked at about 475 nm, due to a singlet-singlet excited state absorption. The ESA becomes slightly narrower in about 0.4 ps, as effect of a rapid excited state relaxation process. In about 9 ps the spectral shape evolves: the band peaked at 475 nm narrows even further and a second peak develops at 680 nm. Comparison with the triplet spectrum reported in the literature allows assigning this component as the triplet-triplet absorption spectrum of **PQ**, thus implying that the molecule undergoes a very fast intersystem crossing (ISC), which occurs in about 9 ps. The

rate of triplet formation can be inferred also looking at the kinetic traces reported in Figure S41, in particular looking at the rise time of the band at 680 nm.

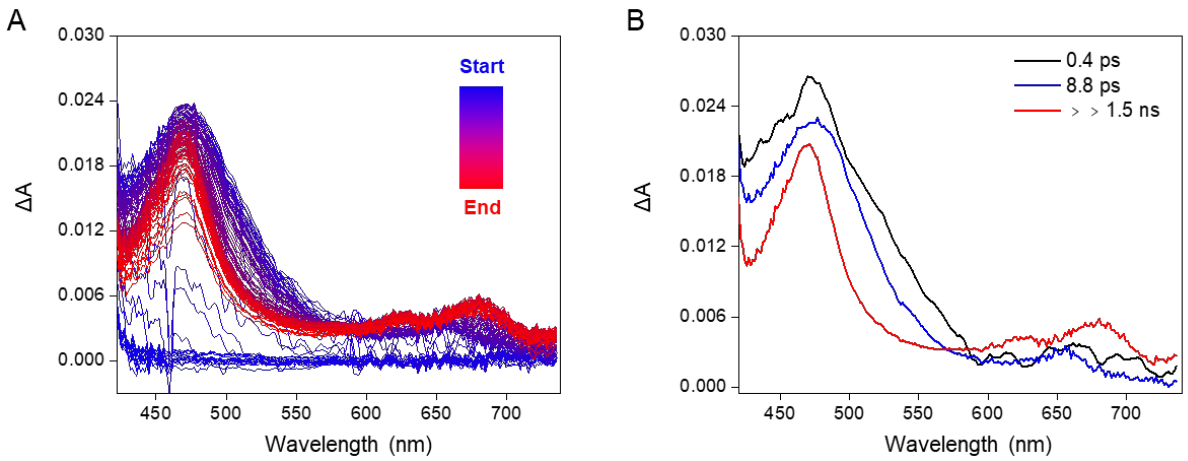

Fig. S40. A) Transient absorption spectra and **B)** EADS obtained from global analysis of the transient absorption data recorded for **PQ** in MeCN upon excitation at 400 nm.

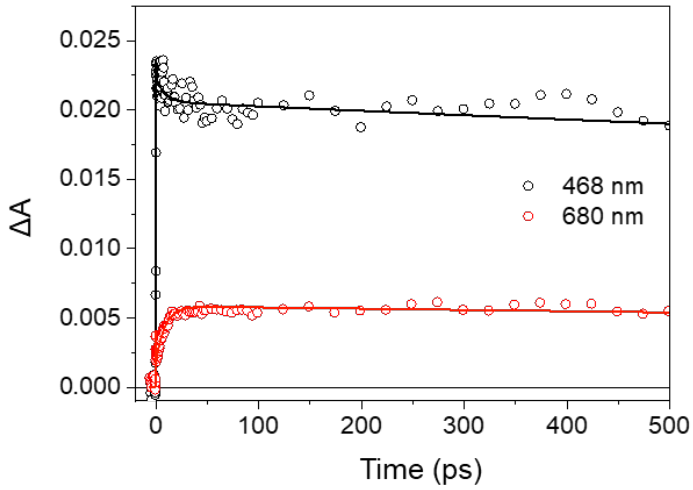

Fig. S41. Kinetic traces taken at 468 and 680 nm for **PQ** in MeCN with the fit obtained from global analysis

Ultrafast transient absorption spectra and significant kinetic traces measured for **PQ-3TP** and **PQ-3DiTP** are shown in Figure S42 and S43.

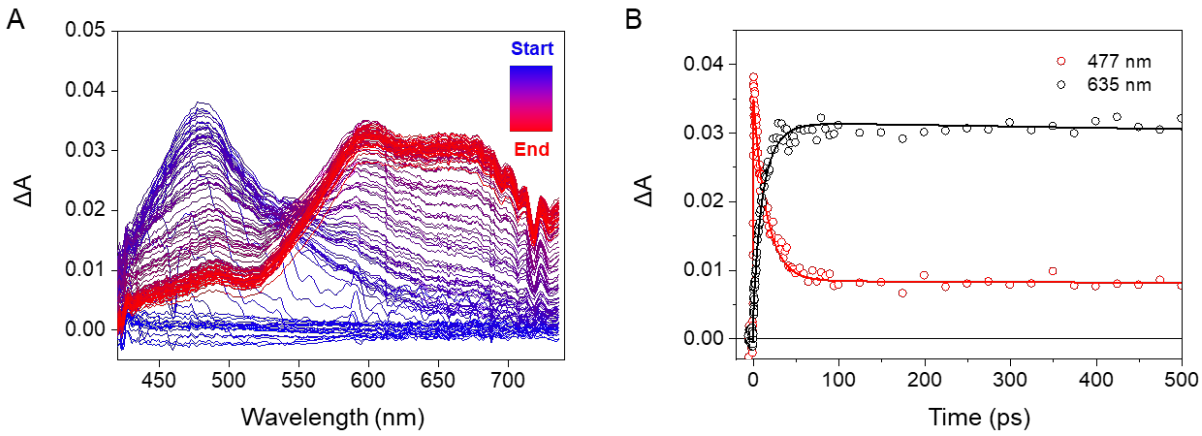

Fig. S42. A) Transient absorption spectra and **B)** Kinetic traces taken at 477 and 635 nm for **PQ-3TP** in MeCN with the fit obtained from global analysis

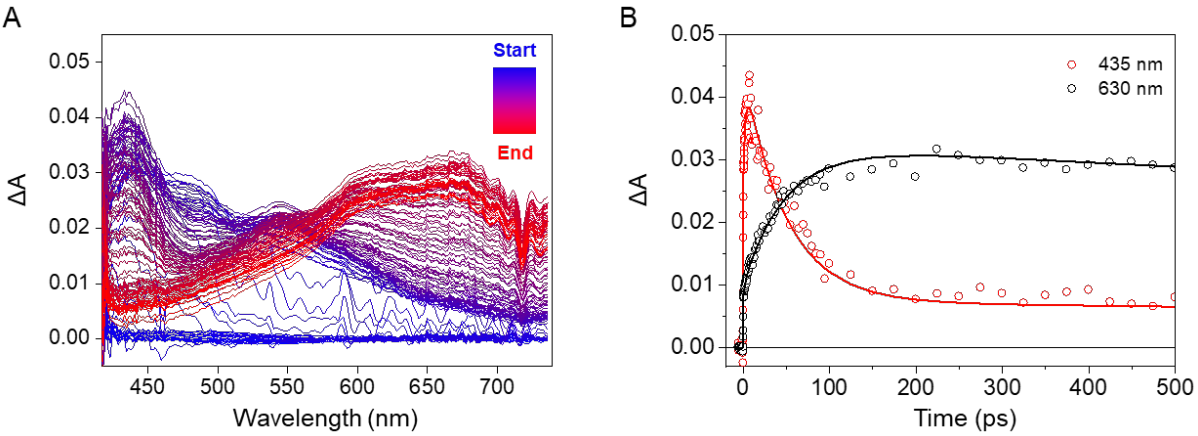

Fig. S43. A) Transient absorption spectra and **B)** Kinetic traces taken at 435 and 630 nm for **PQ-3DiTP** in MeCN with the fit obtained from global analysis

4.5. Nanosecond Transient Absorption Spectroscopy

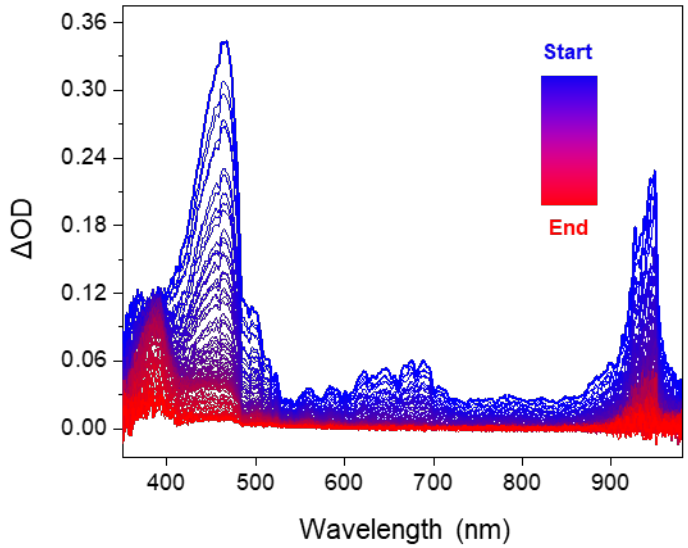

Fig. S44. Nanosecond transient absorption of **PQ** in MeCN at room temperature under N_2 atmosphere. The sample was irradiated at 400 nm upon which the spectrum was recorded in steps of 2 μs increasing delay.

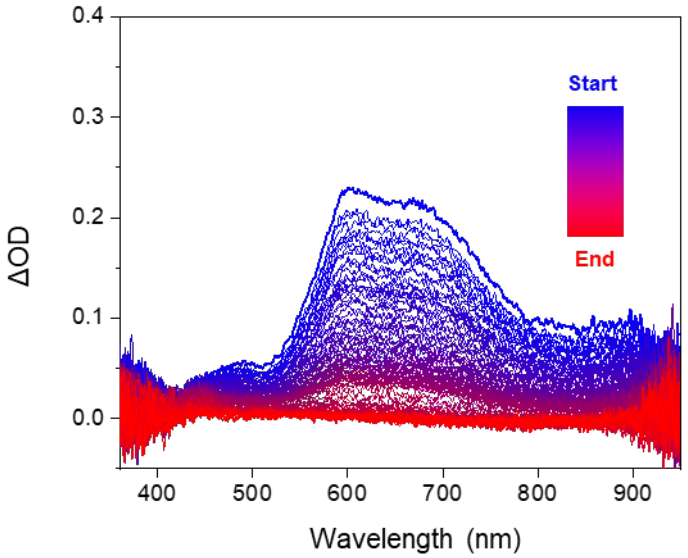

Fig. S45. Nanosecond transient absorption of **PQ-3TP** in MeCN at room temperature under N_2 atmosphere. The sample was irradiated at 400 nm upon which the spectrum was recorded in steps of 2 μs increasing delay.

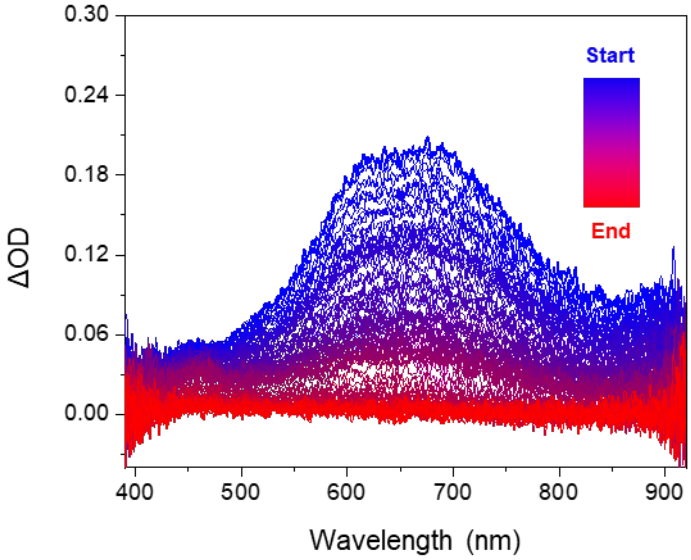

Fig. S46. Nanosecond transient absorption of **PQ-3DiTP** in MeCN at room temperature under N_2 atmosphere. The sample was irradiated at 400 nm upon which the spectrum was recorded in steps of 2 μs increasing delay.

4.6. Power dependance of the triplet lifetimes

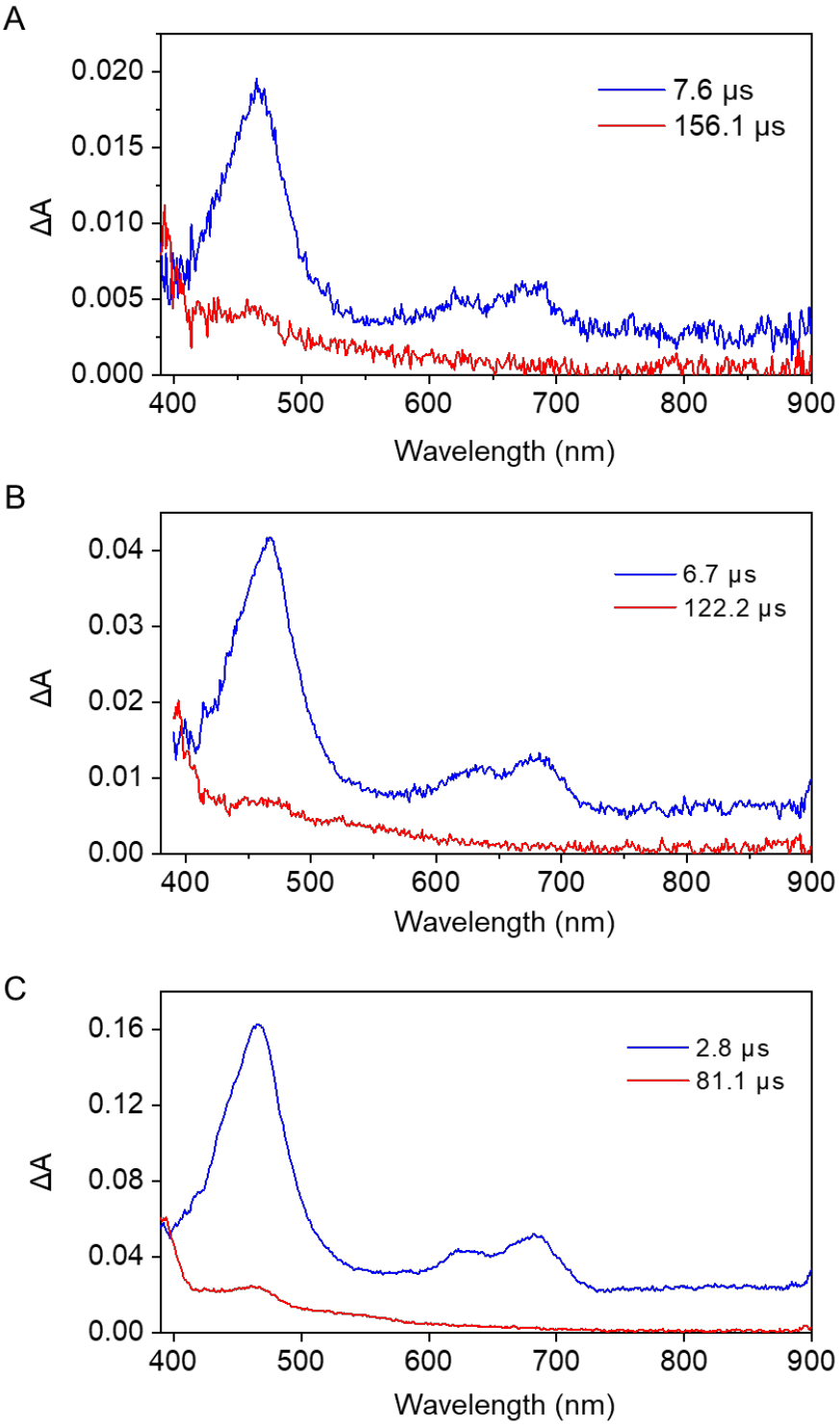

Fig. S47. EADS obtained from global analysis of the nanosecond transient absorption spectra of **PQ** in MeCN at room temperature under N_2 atmosphere, excited at 400 nm at different excitation powers (0.04, 0.10, and 0.36 mJ/pulse, for **A**, **B**, and **C** respectively)

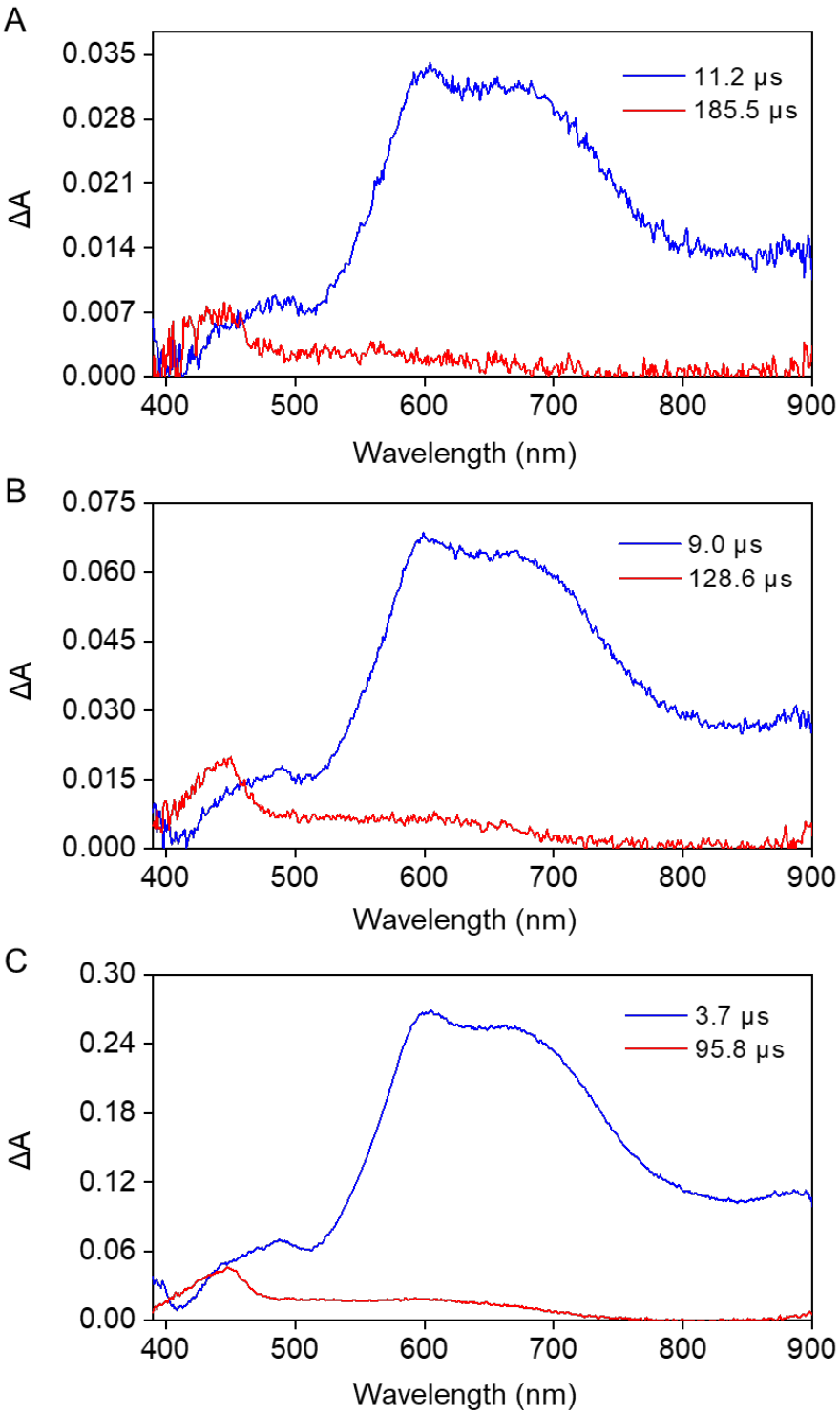

Fig. S48. EADS obtained from global analysis of the nanosecond transient absorption spectra of **PQ-3TP** in MeCN at room temperature under N_2 atmosphere, excited at 400 nm at different excitation powers (0.03, 0.106 and 0.34 mJ/pulse, for **A**, **B**, and **C** respectively)

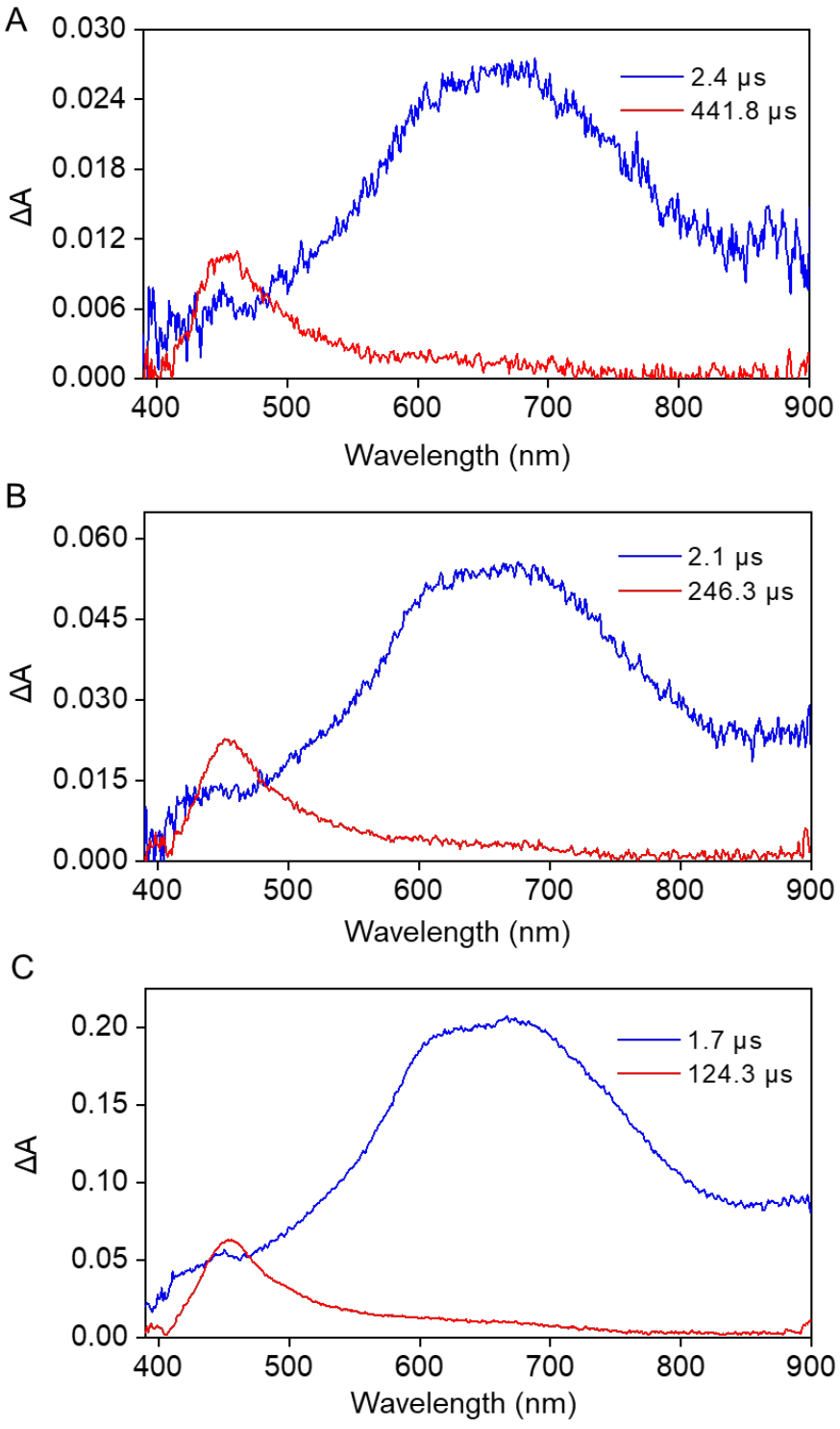

Fig. S49. EADS obtained from global analysis of the nanosecond transient absorption spectra of **PQ-3DiTP** in MeCN at room temperature under N_2 atmosphere, excited at 400 nm at different excitation powers (0.03, 0.08, and 0.30 mJ/pulse, for **A**, **B**, and **C** respectively)

5. Computational analysis

5.1. Symmetry

For our calculations we initially made use of the symmetry of the **PQ** (C_{2v}), **PQ-3TP** (C_s) and **PQ-3DiTP** (C_{2v}). In these symmetry groups the $^3n\pi^*$ and $^3\pi\pi^*$ states have a different symmetry and can thus be optimized independently at the UDFT level. Geometry optimization of the electronic ground state and of these two triplet states in general led to a harmonic force field with one or more small imaginary frequencies along out-of-plane modes. Non-planar geometry optimization along such modes led to a lower energy, but these energy lowering were so small that the potential energy surface along these modes in practice features a double minimum potential with the vibrationless level above the barrier formed by the high-symmetry geometry. This implies that for all practical purposes the molecule still retains the full symmetry. Calculations of absorption spectra have been performed at optimized non-planar triplet geometries to confirm that these spectra for all practical purposes are identical to the ones calculated for the high-symmetry geometry.

5.2. Excitation energies of lower excited singlet states.

For **PQ** it has been well established that the $^1n\pi^*$ and $^1\pi\pi^*$ states are both vertically as well as adiabatically S_1 and S_2, respectively. In order to confirm that such is also the case for **PQ-3TP** and **PQ-3DiTP** and to determine to what extent the energy gap between these two states is changed upon substitution, we report in Table S1 the vertical and adiabatic excitation energies of the lowest $^1n\pi^*$ and $^1\pi\pi^*$ states of **PQ**, **PQ-3TP** and **PQ-3DiTP**. This Table shows that the ordering of the two states as it is in **PQ** remains the same in the two substituted compounds, albeit that the energy gap between the two states is slightly reduced upon substitution.

Table S1. Vertical and adiabatic electronic excitation energies (eV) of the $^1n\pi^*$ and $^1\pi\pi^*$ states of **PQ**, **PQ-3TP** and **PQ-3DiTP** obtained at the M06-2X/6-31+G*/PCM(acetonitrile) level.

	$^1n\pi^*$ (vertical)	$^1\pi\pi^*$ (vertical)	$^1n\pi^*$ (adiabatic)	$^1\pi\pi^*$ (adiabatic)
PQ	2.52	3.25	2.48	2.85
PQ-3TP	2.53	3.09	2.49	2.78
PQ-3DiTP	2.54	2.98	2.50	2.71

5.3. Comparison with previous studies.

In a previous time-resolved Resonance Raman spectroscopy study on **PQ** dissolved in acetonitrile,[17] it was argued that the 450-500 nm band should be assigned to absorption from the $^3\pi\pi^*$ state and the 600-700 nm band to absorption from the $^3n\pi^*$ state. This was based on the dependence of these two bands on the polarity of the solvent, and on the conclusion that the transitions from the $^3n\pi^*$ and $^3\pi\pi^*$ states occur to different higher-lying triplet states. Our calculations do not confirm the latter conclusion. They show that the 400-500 nm band is present in the absorption spectrum of both triplet states and involves a transition to the same higher-lying $^3\pi\pi^*$ state. The observation that in apolar solvents the 600-700 nm band is not noticed is consistent with a reversal of the order of the two states in apolar solvents as a result of which on a hundreds of nanosecond timescale the $^3\pi\pi^*$ state is very likely to be depopulated or at least much less populated than in polar solvents. Finally, the analysis of the TR^3 spectra obtained at 470 and 680 nm assumed that the 470 nm band only is associated with triplet-triplet absorption of **PQ**. The long-time behavior of the ns transient absorption spectra as depicted in Figures S44 and S47 show, however, apart from the band at 390 nm that was previously assigned already to the ketyl radical, also absorption in the 470 nm region, which most logically is also associated with an electronic transition of the ketyl radical. Such a conclusion is supported by previously reported transient absorption spectra of the ketyl radical in a variety of

solvents.[18] We thus believe that some caution should be taken with the analysis of the results of the TR^3 experiments.

6. References

1 L. N. Lameijer, S. Budzak, N. A. Simeth, M. J. Hansen, B. L. Feringa, D. Jacquemin and W. Szymanski, *Angew. Chem. Int. Ed.*, 2020, **59**, 21663–21670.
2 J. J. Snellenburg, S. P. Laptenok, R. Seger, K. M. Mullen and I. H. M. van Stokkum, *J. Stat. Softw.*, 2012, **49**, 1–22.
3 Y. Zhao and D. G. Truhlar, *Theor. Chem. Acc.*, 2008, **120**, 215–241.
4 R. Ditchfield, W. J. Hehre and J. A. Pople, *J. Chem. Phys.*, 1971, **54**, 724–728.
5 F. Weigend and R. Ahlrichs, *Phys. Chem. Chem. Phys.*, 2005, **7**, 3297–3305.
6 H. S. Yu, X. He, S. L. Li and D. G. Truhlar, *Chem. Sci.*, 2016, **7**, 5032–5051.
7 T. H. Dunning, *J. Chem. Phys.*, 1989, **90**, 1007–1023.
8 J.-D. Chai and M. Head-Gordon, *Phys. Chem. Chem. Phys.*, 2008, **10**, 6615–6620.
9 M. J. Frisch, G. W. Trucks, H. B. Schlegel, G. E. Scuseria, M. A. Robb, J. R. Cheeseman, G. Scalmani, V. Barone, G. A. Petersson and H. Nakatsuji, *Wallingford CT*.
10 K. Lang, L. Davis, S. Wallace, M. Mahesh, D. J. Cox, M. L. Blackman, J. M. Fox and J. W. Chin, *J. Am. Chem. Soc.*, 2012, **134**, 10317–10320.
11 J. Li, H. Kong, L. Huang, B. Cheng, K. Qin, M. Zheng, Z. Yan and Y. Zhang, *J. Am. Chem. Soc.*, 2018, **140**, 14542–14546.
12 T. D. Svejstrup, A. Chatterjee, D. Schekin, T. Wagner, J. Zach, M. J. Johansson, G. Bergonzini and B. König, *ChemPhotoChem*, 2021, **5**, 808–814.
13 Y. Fu, H. Helbert, N. A. Simeth, S. Crespi, G. B. Spoelstra, J. M. van Dijl, M. van Oosten, L. R. Nazario, D. van der Born, G. Luurtsema, W. Szymanski, P. H. Elsinga and B. L. Feringa, *J. Am. Chem. Soc.*, 2021, **143**, 10041–10047.
14 Y. Fu, N. A. Simeth, R. Toyoda, R. Brilmayer, W. Szymanski and B. L. Feringa, *Angew. Chem. Int. Ed.*, 2023, **62**, e202218203.
15 N. A. Simeth, S. Kobayashi, P. Kobauri, S. Crespi, W. Szymanski, K. Nakatani, C. Dohno and B. L. Feringa, *Chem. Sci.*, 2021, **12**, 9207–9220.
16 K. Stranius and K. Börjesson, *Sci. Rep.*, 2017, **7**, 41145.
17 V. R. Kumar, N. Rajkumar, F. Ariese and S. Umapathy, *J. Phys. Chem. A*, 2015, **119**, 10147–10157.
18 P. A. Carapellucci, H. P. Wolf and K. Weiss, *J. Am. Chem. Soc.*, 1969, **91**, 4635–4639.